LAWRENCE
LIVERMORE
NATIONAL
LABORATORY

LLNL-JRNL-412685

Strong Links Between Teleconnections and Ecosystem Exchange Found at a Pacific Northwest Old-Growth Forest from Flux Tower and MODIS EVI Data

S. Wharton, L. Chasmer, M. Falk, K. T. Paw U

May 1, 2009

Global Change Biology

Strong Links between Teleconnections and Ecosystem Exchange Found at a Pacific Northwest Old-Growth Forest from Flux Tower and MODIS EVI Data

Sonia Wharton[1*], Laura Chasmer[2], Matthias Falk[3], Kyaw Tha Paw U[1]

[1]Atmospheric Science, University of California, Davis, California, USA; [2]Cold Regions Research Centre, Wilfrid Laurier University, Waterloo, Ontario, Canada; [3]Land, Air, and Water Resources, University of California, Davis, California, USA

Corresponding author now at: Atmospheric, Earth and Energy Division, Lawrence Livermore National Lab, P.O. Box 808, L-103, Livermore, CA 94551, USA, Tel. ++1-925-422-9295, email: wharton4@llnl.gov

LLNL-JRNL-412685

Keywords: *AmeriFlux, old-growth forest, eddy covariance, net ecosystem exchange, interannual variability, teleconnection patterns, ENSO, EVI*

Abstract

Variability in three Pacific teleconnection patterns are examined to see if net carbon exchange at a low-elevation, old-growth forest is affected by climatic changes associated with these periodicities. Examined are the Pacific Decadal Oscillation (PDO), Pacific/North American Oscillation (PNA) and El Niño-Southern Oscillation (ENSO). We use nine years of eddy covariance CO_2, H_2O and energy fluxes measured at the Wind River AmeriFlux site, Washington, USA and eight years of tower-pixel remote sensing data from the Moderate Resolution Imaging Spectroradiometer (MODIS) to address this question. We compute a new Composite Climate Index (CCI) based on the three Pacific Oscillations to divide the measurement period into positive- (2003 and 2005), negative- (1999 and 2000) and neutral-phase climate years (2001, 2002, 2004, 2006 and 2007). The forest transitioned from an annual net carbon sink (NEP = + 217 g C m^{-2} $year^{-1}$, 1999) to a source (NEP = - 100 g C m^{-2} $year^{-1}$, 2003) during two dominant teleconnection patterns. Net ecosystem productivity (NEP), water use efficiency (WUE) and light use efficiency (LUE) were significantly different ($P < 0.01$) during positive (NEP = - 0.27 g C m^{-2} day^{-1}, WUE = 4.1 mg C / g H_2O, LUE = 0.94 g C MJ^{-1}) and negative (NEP = + 0.37 g C m^{-2} day^{-1}, WUE = 3.4 mg C / g H_2O, LUE = 0.83 g C MJ^{-1}) climate phases. The CCI was linked to variability in the MODIS Enhanced Vegetation Index (EVI) but not to MODIS Fraction of absorbed Photosynthetically Active Radiation (FPAR). EVI was highest during negative climate phases (1999 and 2000) and was positively correlated with NEP and showed potential for using MODIS to estimate teleconnection-driven anomalies in ecosystem CO_2 exchange in old-growth forests. This work suggests that any increase in the strength or frequency of ENSO coinciding with in-phase, low frequency Pacific oscillations (PDO and PNA) will likely increase CO_2 uptake variability in Pacific Northwest conifer forests.

1. Introduction

Changes in climate due to either global warming or natural variability may have large and prolonged influences on the terrestrial carbon cycle (Betts *et al.*, 2004; Cox *et al.*, 2004). Large-scale atmospheric circulations affect regional ocean temperatures (Bony *et al.*, 1997; Chuck *et al.*, 2005), and the location of upper-tropospheric jet streams (Chen, 1982; Esbenson, 1984). They also influence the location and severity of synoptic atmospheric pressure systems, which impact regional weather over land (van Loon & Rogers, 1981; Wallace & Gutzler, 1981; Bell & Basist, 1994; Hurrell, 1995, 1996). The temporal correlations in weather events between two distant locations are called teleconnection patterns. Interest in teleconnection patterns crosses over to the terrestrial carbon-cycle community because they are often associated with end-member (anomalous) weather conditions to which ecosystems are exposed.

Terrestrial ecosystems along the western coast of North America are particularly prone to variations in climate via the eastward movement of weather patterns caused by interrelated equatorial and extratropical ocean-atmospheric oscillations (Mote *et al.,* 2003). Atmospheric teleconnection patterns prevalent along the western coast of North America include the Pacific Decadal Oscillation (PDO), the Pacific/North American Oscillation (PNA) and the El Nino-Southern Oscillation (ENSO). ENSO typically transitions from a warm phase (El Niño) to a cool phase (La Niña) every 2 to 7 years in the equatorial Pacific Ocean. The impact of ENSO is felt in the extratropics through increased (El Niño) or decreased (La Niña) ocean temperature stratification and surface winds, and the associated strengthening (El Niño) or weakening (La Niña) of the Aleutian low. The PDO is described as the dominant mode of low-frequency (inter-decadal) variability in the North Pacific Ocean. A characteristic feature of the PDO is that sea surface temperatures (SST) normally remain consistently above or below the long-term average for two to three decades (Mantua & Hare, 2002). The PNA is a second source of low frequency variability in the Northern Hemisphere extratropics and major phase shifts occur roughly every 10 years (Wallace & Gutzler, 1981). Positive or warm PNA phases are associated with an intensified Aleutian low pressure cell so that warmer air is transported northward along the western coast of North America. In the Pacific Northwest region of North America, warm phases of ENSO, PDO and PNA are associated with warmer and drier winters while cool phases bring cooler, wetter weather to the region (Mote *et al.*, 2003).

The influence of teleconnection patterns and associated weather on vegetation carbon exchange has been previously observed in western North America. Carbon flux studies indicate that western conifer forests have the potential to become weaker or stronger sinks or sources of atmospheric CO_2 during strong ENSO leading modes (e.g., Goldstein *et al.*, 2000; Morgenstern *et al.*, 2004; Schwalm *et al.*, 2007). At a temperate, Douglas-fir forest in British Columbia, Canada, Morgenstern *et al.* (2004) found that fluctuations in net ecosystem production (NEP) were linked to air temperature anomalies during the 1997-1999 ENSO period. During the El Niño (1997-1998) event, Morgenstern *et al.* (2004) observed lower annual NEP (i.e., reduced net carbon uptake) in a 56-year old Douglas-fir forest than during the following La Niña phase in 1999. Primary differences in annual NEP were attributed to higher ecosystem respiration (R_{eco}) during the warm El Niño and attenuated respiration during the cooler La Niña. Tree growth along western North America is sensitive to periodic climate variations because net primary production (the excess of gross primary production (GPP) to autotrophic respiration) is related to air temperature and precipitation anomalies (Graumlich *et al.*, 1989; Gedalof & Smith, 2001; Case & Peterson, 2005).

Forest carbon exchange sensitivity to variation in teleconnection patterns may not level off with increasing tree age. A small but robust number of long-term eddy covariance studies have been made in old-growth forests (Hollinger *et al.*, 1994; Anthoni *et al.*, 2002; Knohl *et al.*, 2003; Loescher *et al.*, 2003; Paw U *et al.*, 2004; Desai *et al.*, 2005; Dunn *et al.*, 2007) including a few in locations that provide insight on how teleconnection patterns influence old-growth forest carbon exchange. High variability in annual NEP at La Selva, an old-growth forest in Costa Rica, has been linked to ENSO phase changes (Loescher *et al.*, 2003). Net carbon uptake by the wet, tropical forest was at a 3-year low (NEP = -5 to +133 g C m^{-2} $year^{-1}$) during the 1998 El Niño and substantially increased (NEP = +153 to +314 g C m^{-2} $year^{-1}$) the next year during a cool La Niña. Tree ring measurements at La Selva provide an even longer time series of tree growth variability. These biometric data suggest that net primary production in the tropical, old-growth forest has decreased over the last two decades, primarily in response to an increasing frequency in El Niño events (Clark *et al.*, 2003). In addition, tree ring measurements taken from a Manitoba, Canada old-growth spruce forest indicate a periodicity of approximately 7 years and suggest a link between tree growth and oscillating environmental factors while variation in ring width could not be linked directly to annual changes in temperature and precipitation (Rocha *et al.*, 2006).

Despite the relatively small size (10^5 km^2) of the Pacific Northwest forest biome, significant changes in carbon sequestration in these ecosystems will likely influence the North American carbon budget. Pacific Northwest evergreen forests are estimated to have the highest levels of carbon sequestration in North America (Turner *et al.*, 1995) and possibly the world (Franklin & Waring, 1980; Smithwick *et al.*, 2002), and have the highest potential for future carbon uptake of any terrestrial ecosystem (Schimel *et al.*, 2000). Mature (> 100 years old) forests contain the bulk of the Pacific Northwest vegetation carbon stock and in a study by Law *et al.* (2003) were found to store 85% of the total biomass carbon stock in central Oregon. The conventional ecological paradigm (e.g., Odum, 1965) predicts that after a serious disturbance approximately 500 years ago (catastrophic fire), Wind River was initially a strong carbon source to the atmosphere that rapidly shifted into a sink within a few decades, peaked after some 80 years, and then declined as a sink until reaching present-day carbon equilibrium (DeBell & Franklin, 1987; Franklin & DeBell, 1988). Following this hypothesis, any significant changes in carbon sequestration at Wind River will be due to local disturbances within the stand (e.g., insect outbreaks, wind throw), and without such events, old growth forest carbon exchange should remain "carbon neutral", i.e., photosynthesis and respiration fluxes are balanced and constant (e.g., Thornton *et al.*, 2002; Law *et al.*, 2004; Trofymow *et al.*, 2008).

In this study, we will utilize three groups of independent measurements: global climate indices, flux tower eddy covariance data and Moderate Resolution Imaging Spectroradiometer (MODIS) vegetation indices to examine the relationship between teleconnection patterns and carbon exchange. The eddy covariance technique has high temporal resolution which enables it to capture carbon exchange variability in forests over time ranges lasting from seconds to years, but because it is a one-point based measurement system, the technique is limited to a spatial resolution of 1 to 2 km or less depending on the instrumentation height. Fortunately, the satellite-derived vegetation indices (e.g., MODIS-derived Enhanced Vegetation Index (EVI)) provide measurements for all of North America at stand-level resolutions (e.g., 0.25 to 1 km), are sensitive to changes in forest canopy structure, and have shown potential for tracking seasonal forest carbon dioxide flux variability in deciduous and some evergreen ecosystems (Rahman *et al.*, 2005).

Our goals of this paper are to:

(1) Identify any relationships between three Pacific teleconnection (PDO, PNA and ENSO) leading modes and local weather at Wind River using historical climate records.

(2) Identify any influence that teleconnection patterns have on old-growth ecosystem exchange (NEP, GPP and R_{eco}) and the mechanistic variables, light use efficiency (LUE) and water use efficiency (WUE).

(3) Identify any variability in the MODIS vegetation indices EVI and fraction of photosynthetically absorbed radiation (FPAR) for the old-growth stand. If MODIS variability is present, we will identify any influence that teleconnection patterns have on Wind River EVI and FPAR.

(4) Identify any relationships between MODIS EVI and FPAR variability and flux tower NEP variability over the nine year measurement period.

If our study finds significant variability in carbon exchange in the oldest forest in the FLUXNET network and we are able to link this variability to teleconnection patterns instead of to local disturbance events, then global climate indices may hold promise for predicting forest carbon sink or source activity across a much wider range of stand ages since old-growth ecosystems are assumed to be the least sensitive to climate variability. Furthermore, if we find teleconnection-driven variability in MODIS EVI and FPAR products for the old-growth canopy and we are able to link that variability to variability in tower measurements of NEP, then we will show promise for using remote sensing data to observe climate-driven changes in carbon sequestration in old-growth forests.

2. Materials and Methods

Statistical methods

All linear models in this analysis are based on the "weighted least-squares" method and were done using the statistical software package Origin 8 (OriginLab Corp., Northampton, MA). Due to relatively small sample sizes, we report the coefficients of determination (R^2) in terms of the adjusted R^2 values. We also report the Spearman's correlation coefficient (r) and one-way ANOVA p-value (P) at a significance level equal to the 99th confidence level ($P < 0.01$).

Site Description

This research was carried out at the Wind River Canopy Crane AmeriFlux research station (45° 49' 13.76" N, 121° 57' 06.88" W, 371 m above sea level) in southern Washington State during the years of 1999-2007. The 85 m tall canopy crane is located in a 500-hectare old-growth, conifer forest in the T.T. Munger Research Natural Area, a protected section of the Gifford Pinchot National Forest. The site has been unmanaged for centuries since originating from a natural fire disturbance. Despite the surrounding complex terrain of the western Cascade Mountains, the forest is located in a relatively flat valley (slope is 3.5%). Maximum micrometeorological fetch reaches approximately 2 km within the homogeneous forest (Paw U *et al.*, 2004). Shaw *et al.* (2004) provide a detailed site description for Wind River. In brief, the two dominant tree species are Douglas-fir (*Pseudotsuga menziesii* (Mirbel) Franco) and western hemlock (*Tsuga heterophylla* (Raf.) Sarg). Secondary tree species include western red-cedar (*Thuja plicata* Donn.), Pacific silver fir (*Abies amibilis* (Dougl.) Forb.), western white pine (*Pinus monticola* Dougl.), noble fir (*Abies procera* Rehd.), and grand fir (*Abies grandis* (Dougl.) Lindl.). Trees within the site range in age from 0 to approximately 500 years old and reach maximum heights of 60 meters. Leaf area index (LAI) has been estimated between 8.2 - 9.2 m^2 m^{-2} (Thomas & Winner, 2000; Parker *et al.*, 2004) and total biomass is estimated at 619 Mg C m^{-2}, of which 221 Mg C m^{-2} is stored in the soil and detritus (Harmon *et al.*, 2004). The local climate is characterized by very wet and mild (1 ºC, mean daily temperature) winters interspersed with a strong, seasonal drought (10% of annual precipitation) and warmer temperatures during the summers (Shaw *et al.*, 2004; Falk *et al.*, 2005).

Carbon and water fluxes

Ecosystem carbon dioxide and water vapor fluxes were measured using eddy covariance (EC) methodology (see Swinbank, 1951; Goulden *et al.*, 1996; Paw U *et al.*, 2000). The EC system consisted of a sonic anemometer (Solent HS, Gill Instruments, Lymington, England, UK) which measured the wind velocity vectors and sonic temperature, and a closed-path infrared gas analyzer (IRGA) (LI-6262 until 2006, LI-7000 after 2006, LI-COR, Lincoln, Nebraska, USA) which measured the concentrations (mixing ratios) of H_2O and CO_2 at 10 Hz. The IRGA and sonic anemometer were mounted on a 5 meter long boom at a height of 67 meters on the crane tower so that the anemometer faced west, the predominant wind direction. Carbon dioxide (μmol CO_2 m^{-2} s^{-1}) and water vapor (mmol H_2O m^{-2} s^{-1}) fluxes were time averaged over 30-minute periods using methods described in Paw U *et al.* (2004) and Falk (2005). Half-hour CO_2 fluxes were further screened for outliers, gap-filled for missing values (using a running-mean approach, Reichstein *et al.*, 2005), and nighttime corrected for erroneous flux measurements taken during low turbulence conditions using a friction velocity (u_*) threshold of 0.3 m s^{-1} (Paw U *et al.*, 2004; Falk, 2005; Falk *et al.*, 2008).

The flux data include a continuous, nine year record starting in January 1999 and ending in December 2007 (31% of the data were missing or removed because of undesired wind directions or heavy precipitation), with all carbon dioxide exchange components integrated to daily, monthly and annual sums. Daily net ecosystem production (NEP) (g C m^{-2} day^{-1}) was calculated as the sum of half-hour carbon dioxide fluxes,

$$NEP = -\sum (F_c + S_c) \tag{1}$$

F_c in Eqn (1) is the direct CO_2 flux measurement from the EC system. The carbon storage flux, S_c, was routinely computed for all half-hours using the mean carbon dioxide concentration at the top of the canopy. The effects of S_c on monthly and annual NEP sums were found to be negligible because S_c integrated to zero over monthly and annual time scales (Falk, 2005). F_c fluxes are negative when more carbon dioxide enters the plant canopy than is released to the atmosphere as a result of ecological processes. NEP, by definition, is positive when the net transport of carbon dioxide is downward into the canopy.

Daily ecosystem respiration (g C m^{-2} day^{-1}), R_{eco}, was estimated based on an empirically derived, exponential fit ($a \cdot e^{b \cdot T_{a2}}$) between half-hour, nighttime F_c data taken under sufficient atmospheric mixing (when u_* is > 0.3 m s^{-1}) and the 2 meter air temperature, Ta_{02}, and corrected for moisture limitations in the summer months (Falk *et al.*, 2005):

$$R_{eco} = \sum ((y_o + c * \exp(d * \theta_v)) * (a * \exp(b * Ta_{02})) \tag{2}$$

The first term on the right hand side of Eqn (2) is a respiration attenuation function which is activated when soil water content (θ_v) drops below 0.2 m^3 m^{-3} and prevents the overestimation of ecosystem respiration on warm, dry summer days. All equation parameters (a-d, y_o) were empirically derived from nighttime flux data collected during periods when u_* > 0.3 m s^{-1}. For further details on the derivation of the respiration expression see Falk *et al.* (2005).

Daily NEP and R_{eco} sums were used to estimate gross primary production (GPP) (g C m^{-2} day^{-1}),

$$GPP = NEP + R_{eco} \tag{3}$$

In Eqn (3), R_{eco} and GPP are always positive fluxes and GPP is greater than R_{eco} if NEP is positive. Monthly and annual NEP, R_{eco}, and GPP estimates were calculated from the sum of their corresponding daily fluxes (Falk *et al.*, 2008). In this study we calculated annual NEP based on the Julian calendar year (January through December).

Meteorological data

Historical (1950-1977) monthly total precipitation and mean air temperature data were available from the Wind River Meteorological Station (45° 28' 47.99" N, 121° 33' 36" W, 351 m a.s.l.). Daily precipitation and air temperature data were available from 1977 through 2007 at the nearby Carson Fish Hatchery NOAA station (45º 31' 12" N, 121º 34' 48" W; 345.6 m a.s.l). The historical climate date record was used because it captures local temperature and precipitation anomalies during two complete PDO cycles between 1950 and 2007. We normalized the precipitation and air temperature data records based on the historical mean and standard deviation to produce standardized anomalies that could easily be compared to the climate indices. Positive (negative) standardized anomalies indicate wetter (drier) than normal or warmer (cooler) than normal conditions.

At the canopy crane, air temperature and relative humidity (HMP-35C, Vaisala Inc., Helsinki, Finland) and downwelling photosynthetically active radiation (PAR) (190-SB, LI-COR) were measured at heights of 2 m (below canopy) and 70 m (above canopy) along the crane tower. The meteorological measurements were collected as 30-minute averages from January 1999 through December 2007.

VPD and efficiency parameters

The influences of meteorological driving mechanisms on CO_2 and H_2O fluxes are often manifested in efficiency parameters (e.g., WUE and LUE) (Loomis & Williams, 1963; Lemon, 1969; Monteith, 1972, 1977). Above canopy vapor pressure deficit (VPD), light use efficiency (LUE), water use efficiency (WUE), and fraction of intercepted photosynthetically active radiation (FPAR) were derived using a combination of meteorological and eddy covariance instrumentation data.

VPD is an important driver of canopy gas-atmosphere exchange because it influences stomatal conductance and can limit photosynthetic CO_2 uptake and leaf water loss when VPD is high, particularly when soil moisture is limiting (Schulze, 1986). Daily mean VPD was calculated using the half-hourly, 70 meter air temperature and relative humidity data during daylight periods only.

LUE is an estimate of the efficiency in which plants use light for carbon assimilation (Monteith, 1972, 1977). In Eqn (4), we define daily LUE in terms of mass of carbon assimilated (g C) for every megajoule (MJ) of light intercepted by the canopy,

$$LUE = GPP / Q_i \tag{4}$$

Where, GPP is gross primary productivity (g C m^{-2} day^{-1}) and Q_i is intercepted incoming PAR through the canopy (MJ m^{-2} day^{-1}),

$$Q_i = Q_a (1- e^{(-LAI * k)}) \tag{5}$$

In Eqn (5), Q_a is above canopy incident PAR (MJ m^{-2} day^{-1}), LAI = 8.5, and the light extinction coefficient (k) was estimated using the Beer-Lambert law (range = 0.45 to 0.51). Our LUE methodology was adapted from Gower *et al.* (1999).

The fraction of PAR intercepted within the canopy (FPAR) was also estimated from incoming PAR measurements taken above (Q_a) and below (Q_b) the canopy at heights equal to 70 m and 2 m above the ground surface, respectively. Mean midday FPAR was estimated for each day using the half-hour measurements between 1000 and 1500 Pacific Standard Time (PST), Eqn (6),

$$FPAR = 1 - (Q_b / Q_a) \tag{6}$$

Diffuse radiation measurements at the canopy crane were not available for an assessment of any PAR-GPP response curve differences due to direct versus diffuse radiation absorption. Instead, we categorized daily incoming PAR data into dark and cloudy, cloudy, partly cloudy and sunny periods based on an index called the clear sky fraction (CSF), defined in Eqn (7),

$$CSF = Q_a / Q_{amax} \tag{7}$$

CSF was calculated for each day by normalizing midday (1000 through 1500) incoming PAR (Q_a) by the maximum annual midday PAR value (Q_{amax}). CSF by definition ranges from 0 (cloudy, dark sky) to 1 (maximum brightness, clear sky). Here, CSF was used as a proxy for daily diffuse (CSF approaches 0) and direct (CSF approaches 1) radiation conditions. Water use efficiency (WUE) is defined as the total mass of dry matter (mg C) produced by photosynthesis for every gram of water lost by vegetation through transpiration (e.g., Rosenberg *et al.*, 1983). Direct measurements of transpiration (e.g., from sapflow measurements) were not available at the site for this time period. Therefore, the WUE expression was modified to represent the total mass of carbon (mg C) assimilated for every gram of water lost by the ecosystem through evapotranspiration (E_T),

$$WUE = GPP / E_T \tag{8}$$

In Eqn (8), the above canopy latent energy flux was used to calculate E_T for all daylight half-hours when the latent energy flux was greater than zero (Berbigier *et al.*, 2001). A mean midday WUE (mg C / g H_2O) was calculated on a daily basis using the half-hours 1000 through 1500. The E_T data were screened to remove half-hours during and after rainy periods when much of evapotranspiration is water evaporating from the wet canopy.

Teleconnection patterns

The established methodologies describing how the climate indices are calculated are briefly discussed below and are listed in Table 1. We based our annual climate indices on mean autumn-winter-spring values because regional weather anomalies are most highly correlated to climate indices during the rainy season (Mote *et al.*, 2003). The PDO is defined as the leading principle component of North Pacific sea surface temperature variability and has the strongest "climate footprint" in the North Pacific/North American regions (Mantua & Hare, 2002). Our annual PDO index is defined from November through March using autumn of the prior year and winter of the listed year, e.g., 2004 is defined as November 2003 through March 2004. The historical range (1950-2007) for the annual PDO index is -3 to + 3. The PNA index is both a monthly and daily index estimated from rapidly varying atmosphere pressure anomalies over the North Pacific Ocean and is associated with the strength and location of the East Asian jet stream

(Wallace & Gutzler, 1981). Here, we used the winter months of November-March to compute our annual PNA index because the PNA reaches maximum strength around February and has relatively little influence over summer-time temperature variability in North America (Barnston & Livezey, 1987). The annual PNA index range is from -2 to +2. Our study uses the Multivariate ENSO Index (MEI) to describe El Niño and La Niña behavior which is based on six meteorological variables over the tropical Pacific Ocean: sea level pressure, zonal and meridional component of surface wind, SST, surface air temperature, and total cloudiness fraction. The MEI is calculated in the following steps, first, the individual meteorological variables are spatially filtered into clusters, second, the total variance of each variable is normalized, and third, the first principle component on the co-variance matrix of the combined variables is extracted (Wolter & Timlin, 1993). All seasonal MEI values are then standardized with respect to each season and to the historical reference period (Wolter & Timlin, 1993) and annual MEI magnitudes range from -3 to +3. MEI is calculated as a bimonthly index and correlations between MEI and the alternative Southern Oscillation Index (SOI) are high: 0.8 to 0.9 (Wolter & Timlin, 1998). In this paper, an annual MEI was computed based on December-February values. All three indices (PDO, PNA and MEI) are assigned positive values during positive or warm modes and negative values during negative or cool modes by the data providers listed in Table 1. Between 1950 and 2007, the three indices were positively correlated to each other at the significance level ($P < 0.01$). Coefficients of determination (R^2) were 0.54 (PDO and MEI), 0.38 (PDO and PNA), and 0.27 (PNA and MEI) during the winter months. Table 2 shows the frequency of in-phase PDO, PNA and MEI events. Between 1950 and 2007, the three indices were concurrently in a negative phase 30% of the time and in a positive phase 25% of the time.

Due to a high degree of autocorrelation between the three oscillations, we chose to concentrate on their in-phase, additive effects and created a new climate index called the "Composite Climate Index" (CCI). The CCI incorporates the PDO, PNA and MEI magnitudes into a single index by summating the three individual indices. Our annual CCI values ranged from -1.9 (designated as a strong negative phase year) to +3.0 (designated as a strong positive phase year) during the 1999-2007 flux measurement period. Years with CCI values below -1.0 were classified as negative phase years (1999, 2000), years with CCI values above +1.0 were classified as positive phase years (2003, 2005), and years with CCI values between -1.0 and +1.0 were classified as neutral phase years (2001, 2002, 2004, 2006, 2007). The Composite Climate Index was also calculated on a monthly basis to examine the relationships between the climate phases, carbon fluxes and mechanistic variable anomalies over shorter time periods.

MODIS

Vegetation indices derived from the MODIS spectroradiometer onboard the Terra satellite were subsetted and downloaded for a 2.25 km x 2.25 km area centered on the Wind River Canopy Crane AmeriFlux site (http://daac.ornl.gov/MODIS/). The vegetation indices included 8-day Fraction of absorbed Photosynthetically Active Radiation (FPAR) (1 km resolution, MOD15A2, Collection 5.0) and 16-day Enhanced Vegetation Index (EVI) (250 m resolution, MOD13A2, Collection 5.0) collected from 2000 through 2007. Tower-centered and surrounding pixels which contained large index differences above or below the previous and following 8- and 16-day periods were assumed to be influenced either by other land cover types, issues with MODIS FPAR/EVI inputs, or contamination by atmospheric constituents (e.g. Tian *et al.* 2002), and were removed from the analysis (14% of the data). Here, we used EVI and

FPAR data for the months of May through October to minimize reflectance errors due to snow cover and clouds during the winter months.

The MODIS FPAR product is an estimate of the amount of downwelling radiation that is absorbed by the plant canopy and was derived using MODIS atmospherically corrected spectral reflectance bands and the Multi-angle Imaging Spectroradiometer (MISR). These are used to estimate the bi-directional reflectance factors (Knyazikhin *et al.*, 1999; Myneni *et al.*, 2002). The EVI is an index commonly used for enhancing the absorbed and reflective parts of the radiative spectrum typically as a result of above ground vegetation. The EVI uses the near infrared and red bands, and near infrared and blue bands with a gain factor and a canopy background adjustment (Huete *et al.*, 1999). This reduces background errors in the vegetation index due to soil and atmospheric effects whilst remaining sensitive to a high biomass density. The EVI has been applied to examine phenological and land cover changes, and structural attributes of vegetative canopies (e.g., Huete *et al.*, 1999).

3. Results

Climatic fluctuations

The historical (1950-2007) average for Wind River is 8.83 °C mean annual air temperature and 2366 mm total water-year (October through September) precipitation. During the flux measurement period (1999-2007), positive CCI years were 0.49 °C warmer and 270 mm drier than normal, while negative CCI years were 0.26 °C cooler and 467 mm wetter than normal. Neutral CCI years were slightly warmer (+ 0.13 °C) and drier (- 72 mm) than normal. Fig. 1 shows a time series of the annual precipitation and temperature anomalies (normalized by the mean and standard deviation) and the annual global climate indices over the historical climate record. Negative climate phases were most often associated with positive (greater than normal) precipitation anomalies, while drier years occurred more frequently during positive climate phase events ($R^2 = 0.18$, $P < 0.01$). The relationship between air temperature and climate phase was not significant ($R^2 = 0.05$, $P > 0.01$), although cooler temperatures occurred more often during negative climate phases. The largest historical temperature and precipitation anomalies occurred when the three climate indices were all in-phase (Table 3). From 1950-2007, CCI magnitudes ranged from - 4.71 (1957) to + 4.65 (1998), had a Gaussian distribution (Shapiro-Wilk test for normality), a mean around zero (-0.05) and a standard deviation of 2.1 at the 95th confidence level (Fig. 2).

Relationship between climate indices, local meteorology and carbon fluxes

Figure 3 shows the annual PDO, PNA and MEI time series data as well as the CCI values and eddy covariance NEP estimates. The CCI was able to capture the observed trends in the NEP data series. It is important to notice that NEP in Figure 3 is plotted as – NEP (i.e., net ecosystem exchange). This was done so that net carbon uptake years have the same sign notation as negative climate phase years which makes it easier to visually identify a trend between the two time series. From 1999 through 2003, the climate indices transitioned to a more positive state whilst annual carbon uptake at the old-growth forest declined and the forest was a significant source of carbon in 2003. Since 2003, the climate indices have transitioned back to more negative phases and carbon uptake has increased over the last couple of years compared to the 2003-2005 annual NEP average.

During the nine-year flux measurement period, water-year precipitation ranged from 1269 mm (October 2000- September 2001) to 2834 mm (October 1998 - September 1999), annual mean temperature from 8.4 ºC (2000) to 9.7 ºC (2003), and growing season mean temperature from 12.3 ºC (1999) to 13.9 ºC (2004). The negative phase years were cooler than normal during the spring (March, May) and summer (July) months, while positive climate phase temperatures were usually warmer except during mid-winter (Fig 4a). Fig. 4b shows differences in the measured vapor pressure deficit (VPD). Here, July and August are highlighted to show important inter-seasonal variations when dominant negative or positive teleconnection patterns occurred. VPD was lower during mid-summer (July) in cool phase years, coinciding with lower air temperatures. Although, the mean air temperature in August was similar amongst all years, warm phase years had markedly higher VPD indicating the presence of drier, continental air masses.

Fig. 5a shows that there is significant relationship ($R^2 = 0.55$, $P < 0.01$) between annual NEP and annual CCI and increased carbon uptake is associated with more negative climate phases. The linear model statistics are listed in Table 4 for Fig. 5 as well as all of the "least-squares" regressions. Negative climate phases bring cooler than normal air temperatures and higher than normal winter precipitation amounts. Fig. 5b shows that the relationship between monthly CCI and monthly NEP anomalies (deviations from the 1999-2007 mean) has more scatter (R^2 = 0.34) than the annual relationship but the relationship is significant ($P < 0.001$). Although the climate indices are not perfect predictors for annual ecosystem CO_2 sink/source strength, they do come close to estimating yearly NEP. The standard error between measured annual NEP and the climate index-predicted NEP (based on a linear model with 1999-2007 data) was 44 g C m^{-2} $year^{-1}$ and is of the same order of magnitude as the uncertainty in the eddy covariance NEP measurements (± 32 to 54 g C m^{-2} $year^{-1}$). GPP anomalies are plotted against the Composite Climate Index in Fig. 6 on both annual (R^2 = 0.64, $P > 0.01$) and monthly time scales (R^2 = 0.22, $P < 0.001$). While increased carbon uptake (NEP) was associated with negative climate phases in Fig. 5, GPP was higher during positive phases (Fig. 6). Ecosystem respiration anomalies are also positively related to the CCI on annual (R^2 = 0.75, $P < 0.01$) and monthly time scales (R^2 = 0.33, $P < 0.001$). Increased (decreased) respiration was associated with positive (negative) climate phases (Fig. 7).

Seasonal carbon sink-to-source transition

In Fig. 8, monthly NEP (g C m^{-2} $month^{-1}$) is plotted for negative or cool phase years (1999, 2000), positive or warm phase years (2003, 2005) and neutral phase years (2001-2002, 2004, 2006-2007). Notable differences in net carbon exchange occurred during the winter/early spring months (positive phases had on average lower NEP or less net carbon uptake) and summer months (negative phases had on average higher NEP or more net carbon uptake). The boxed section in Fig. 8 highlights a significant event in the NEP data record: the seasonal transition between net carbon sink to net carbon source exchange for the old-growth ecosystem.

During positive phase and neutral phase years this transition to net carbon source occurred in early summer between the months of May and June, but was delayed during the negative phase years. For example, in 1999, the forest ecosystem did not become a net carbon source until September, nearly four months later than normal.

Efficiency parameters

WUE was significantly lower ($P < 0.01$) during negative CCI years than during positive CCI years (Fig 9a). For comparison, water-year precipitation was 467 mm greater than normal in negative years and 270 mm below normal in positive phase years. Mean (± one standard deviation) April-September WUE was 3.4 ± 0.9 mg C / g H_2O (cool phase), 4.1 ± 1.5 mg C / g H_2O (warm phase), and 4.2 ± 0.9 mg C / g H_2O (neutral phase). Growing season LUE was significantly higher ($P < 0.01$) during positive CCI years (0.94 g C MJ^{-1}) than during either negative (0.83 g C MJ^{-1}) or neutral (0.83 g C MJ^{-1}) CCI years. The old-growth forest canopy was most efficient at using light for photosynthesis during positive phase spring months (Fig 9b). Increased early-growing season air temperatures appear to increase LUE in the old-growth canopy. However, LUE during positive phase years is limited during the summer months by high VPD (Fig 4b). In addition, light-response curves (daily GPP versus daily incoming PAR) indicated that GPP saturated at a lower light level (4 to 5 MJ day^{-1}) during negative phase years than during positive phase years (6 to 7 MJ day^{-1}).

Larger climate phase differences in LUE were found after the data were split into cloudy, partly cloudy and sunny days. 1999-2007 daily LUE was negatively correlated with clear-sky fraction, such that LUE was highest on cloudy days (1.72 g C MJ^{-1}) and lowest on clear days (0.55 g C MJ^{-1}). The largest LUE differences were measured during strong teleconnection events in 1999 and 2003: spring (March-May) LUE was 1.74 ± 0.48 g C MJ^{-1} in 1999 and 2.67 ± 0.81 g C MJ^{-1} in 2003 on cloudy days. Higher LUE in spring 2003 could not be attributed to a difference in the number of cloudy days: 33 in 1999 and 37 in 2003. August LUE was 1.02 ± 0.51 g C MJ^{-1} in 1999 and 0.67 ± 0.26 g C MJ^{-1} in 2003, and again LUE differences could not be explained by variations in sky cover. August in 1999 and 2003 had nearly the same number of cloudy/partly cloudy days (14 and 15, respectively) as sunny days (16 and 15, respectively).

Tower-based FPAR measurements differed little (< 2%) during the nine year period even as climate variability was high. 9-year average FPAR was 0.976 ± 0.02 and no seasonal trends were detected. FPAR did increase slightly with both positive CCI phases and warmer air temperatures, suggesting that temperature fluctuations associated with positive climate phases were driving small, but insignificant differences in tower-based FPAR.

MODIS vegetation indices

MODIS-derived EVI was associated with variations in the CCI. Fig. 10 shows a time series plot of monthly CCI (10a), and monthly and mean growing season EVI (10b). Two trends are apparent: (1) the climate phases have become more positive since 1999 and appeared to shift to a warmer phase in 2002, whilst EVI steadily decreased from 2000-2005 and, (2) climate phases may be returning to a cooler or more negative state starting in 2006, and higher EVI magnitudes were observed in 2007. Monthly CCI and EVI (May-October, 2000-2007) were negatively related so that cooler climate phases are associated with higher EVI (Fig. 11a, R^2 = 0.28, $P < 0.001$). Also, monthly NEP anomalies were positively related to monthly EVI fluctuations (R^2 = 0.34) at the significance level ($P < 0.001$). Overall, higher net carbon uptake (more positive NEP) was associated with higher than normal EVI (Fig. 11b). Climate phase-year differences in the MODIS FPAR product were small (< 2%) and insignificant ($P > 0.01$). Average 8-year MODIS-derived FPAR was 0.90 which is less than the tower-based estimate of 0.976 and did not show any climate phase or seasonal trends.

4. Discussion

Our historical (1950-2007) precipitation and mean temperature anomalies during in-phase teleconnection patterns are consistent with independent climatological datasets in the region (e.g., McCabe & Dettinger, 1999; Mote *et al.*, 2003). Negative and positive in-phase PDO and ENSO events have historically differed by 1 ºC for mean air temperature and 20% for total annual precipitation in the Pacific Northwest. Similarly, we reported anomalies of 1 ºC for mean temperature and 30% for precipitation in the historical Wind River climate record during dominant positive and negative climate phases.

We were fortunate that there is an evergreen, conifer forest on Vancouver Island, British Columbia, Canada that has a long-term NEP record (Morgenstern *et al.*, 2004; Humphreys *et al.*, 2006; Schwalm *et al.*, 2007) which overlaps ours at Wind River. Both sites are Douglas-fir forests and are exposed to weather patterns originating over the Pacific Ocean. The NEP records provide an excellent opportunity to compare the results found in this study for an old-growth forest with those at the younger B.C. stand. Annual NEP at the Vancouver Island site matches our observed NEP data at Wind River during the 1998-1999 El Niño-La Niña phase shift. Although the 1998 measurement year at Wind River was incomplete we estimate that the old-growth forest was a small sink or small source of carbon to the atmosphere (NEP = -75 to 50 g C m^{-2} $year^{-1}$) but became a much stronger sink in 1999 (NEP = 217 ± 40 g C m^{-2} $year^{-1}$). Similarly, Morgenstern *et al.* (2004) report higher NEP (328 g C m^{-2} $year^{-1}$) during the 1999 La Niña than during the strong El Niño year of 1998 (296 g C m^{-2} $year^{-1}$). Interestingly, NEP trends at Wind River and Vancouver Island deviate during the next strong El Niño phase in 2003. At Wind River, we measured the lowest NEP (-100 g C m^{-2} $year^{-1}$) on record during an unusually warm 2003 (Δ annual temperature = + 1.0 ºC) while at Vancouver Island, NEP was relatively high in

2003 (318 g C m^{-2} $year^{-1}$) and did not significantly decline until the following year (194 g C m^{-2} $year^{-1}$) (Schwalm *et al.*, 2007). The NEP component fluxes, R_{eco} and GPP, provide clues for why a one year lag in declining NEP appeared between the Wind River and Vancouver Island forests since seasonal weather anomalies at the flux towers were similar. In 2003, respiration fluxes were near average (ΔR_{eco} = -62 g C m^{-2} $year^{-1}$, based on 1998-2004 mean) at Vancouver Island while we estimated the highest annual R_{eco} on record (ΔR_{eco} = +407 g C m^{-2} $year^{-1}$, based on 1999-2004 mean). Record high R_{eco} (ΔR_{eco} = +320 g C m^{-2} $year^{-1}$) was not measured until 2004 at Vancouver Island and corresponded with the 2004 drop in NEP. Smaller phase-year variability was observed in the GPP fluxes at both sites. These two forests have vastly different carbon pools largely due to variations in stand age (450 to 500 years old versus 60 years old) and management history (e.g., 21% of the total carbon pool at Wind River is stored in detritus, Harmon *et al.*, 2004) so the observed delay in declining NEP behavior could be from site differences in respiration rates.

At Wind River, highest annual NEP was associated with negative climate phases while highest GPP and R_{eco} fluxes were associated with positive climate phases. Hence, it is not a substantial increase in GPP which is causing increased carbon uptake during negative climate phases. Instead, higher NEP during negative phases resulted from a substantial decrease in respiration rates which were strongly driven by cooler temperatures in 1999 and 2000 (Falk *et al.*, 2008). The increased carbon sink activity during the negative phase years was primarily due to attenuated respiration fluxes during the cooler than normal summer months. Monthly maximum respiration fluxes did not occur until August during the strong climate phase, although R_{eco} typically peaks in June or early July at the Wind River forest (Falk *et al.*, 2008). GPP fluxes were also smaller during strongly negative CCI periods although the variation in GPP was less than that observed in R_{eco}. Respiration flux anomalies (versus GPP anomalies) appear to be the stronger driver of variability in net ecosystem productivity at our site. Ours is not the first study to suggest that respiration anomalies play a dominant role in net ecosystem exchange (see Valentini *et al.*, 2000). Increased (decreased) NEP has been associated with reduced (increased) respiration fluxes at a number of European and North American FLUXNET sites (Lee *et al.*, 1999; Law *et al.*, 2000; Pilegaard *et al.*, 2003; Morgenstern *et al.*, 2004) including an old-growth Ponderosa pine stand in central Oregon (Schwarz *et al.*, 2004). It is important to consider that most of these studies have concentrated on the effects that temperature and precipitation anomalies have on NEP and while a relationship between respiration and the two environmental variables is often found, GPP is instead strongly influenced by changes in canopy absorbed PAR and VPD. Luyssaert *et al.* (2007) argue that differences in methodology and measurement periods have produced conflicting conclusions on whether respiration or photosynthesis controls NEP. Furthermore, respiration fluxes are not independent of GPP because R_{eco} is strongly influenced by the allocation of photosynthate and decomposition of biomass to the extent where some respiration fluxes, e.g. soil respiration, may be correlated more to GPP than to temperature (Janssens *et al.*, 2001). A link between higher (lower) annual R_{eco} and higher (lower) annual GPP has in fact been strongly established amongst numerous FLUXNET sites (Janssens *et al.*, 2001; Baldocchi, 2008) including Wind River (Falk *et al.*, 2008). Hence, we stress that some caution is warranted when we describe the roles of GPP and R_{eco} behavior on annual NEP during different climate phase events.

In low-elevation forests in the Pacific Northwest, radial growth is limited by low summer precipitation and high summer temperatures and increases with higher winter precipitation (Case & Peterson, 2005). Likewise, the mechanistic variables at Wind River revealed interesting climate-phase related differences during spring and summer months. We found that WUE at the old-growth forest differed from warm phase to cool phase years depending on vegetative water demand and atmospheric humidity. Although our WUE estimates include evaporation as well as transpiration in the E_T measurement we were careful to removed time periods when evaporation was the dominate water vapor flux. During periods with plentiful precipitation and low VPD, water stress is not chronic and trees can “afford” to keep their stomates open during midday hours throughout the summer to optimize photosynthesis because subsequent water loss (transpiration) is replenished from soil water reserves. In this case, WUE will be relatively low because transpiration is not attenuated during the afternoon hours. On the other hand, stomates regulate (limit) the amount of water lost through transpiration when VPD is high (via higher stomatal resistance) and when soil moisture is limiting, typically producing higher WUE during warm and dry conditions. Our WUE findings are consistent with Wind River WUE data reported by Chen *et al.* (2002) during the 1998-1999 ENSO transition. They estimated summer WUE values of 2.7 ± 4.4 mg C / g H_2O in 1998 (El Niño) and 1.0 ± 2.3 mg C / g H_2O in 1999 (La Niña) (Chen *et al.*, 2002). Our 1999 WUE is higher than the number reported by Chen *et al.* (2002) but this is likely due to differences in methodology and averaging periods since the flux data were post-processed independently by both groups. Chen *et al.* (2002) defined WUE in terms of the NEP flux while we define WUE using the GPP flux. Our WUE estimates are closer in magnitude to the range (2 to 5 mg C / g H_2O) reported by Law *et al.* (2002) for evergreen, conifer forest FLUXNET sites. Our variability in WUE at Wind River was nearly 2 mg C / g H_2O which resulted from significant differences in weather conditions (e.g., VPD and air temperature) during positive and negative climate phases. Highest WUE occurred during the most positive CCI year (2003), a period of warmer and near-normal precipitation, and was attributed more to higher GPP than to lower E_T.

LAI is relatively stable at Wind River in lieu any major disturbance event (Thomas & Winner, 2000) so any year-to-year differences in LUE from 1999 to 2007 could not be attributed to significant leaf area change. The higher light saturation point for GPP during the strongest positive CCI year (2003) suggests that warmer spring-time temperatures were driving higher photosynthetic rates with no subsequent evidence of soil water limitations, which would have had the effect of reducing GPP by inducing significant periods of stomatal closure. Higher LUE and a higher saturation point for GPP both indicate that climate conditions were optimal for photosynthesis in the spring of 2003. Mean air temperature was 1 ºC warmer than normal and precipitation was 95% of normal that year.

Our two point-based (2 m and 70 m) measurement of tower FPAR (0.976) was higher than previous vertical PAR-transect estimates (0.92) taken by Parker *et al.* (2002), but we suggest that any overestimation of intercepted PAR is of small concern in this paper since we highlight variability from the mean over absolute values. The tower-based, annual mean FPAR fluctuations were small (< 2 %) suggesting that there were no significant structural canopy changes over the nine years, and agree with observations of no significant disturbances reported within the stand. Small changes (< 3%) in annual FPAR at undisturbed forests are not uncommon and have been reported for a number of European conifer forests (Reichstein *et al.*, 2007). The MODIS-derived FPAR index also did not show significant variability at the tower-pixel scale. On the other hand, we did observe significant climate phase-driven GPP anomalies at the Wind River flux tower. FPAR estimates at evergreen forests may not reflect observed changes in GPP (Reichstein *et al.*, 2007) and it is not uncommon for MODIS to underestimate

FPAR at high LAI sites (Turner *et al.*, 2005). This is because the physiological controls over photosynthesis (e.g., stomatal control, enzyme activity) have little effect on the MODIS FPAR product (Reichstein *et al.*, 2007).

In contrast, we were able to detect MODIS-derived EVI variability at the tower-pixel level and link this to climate anomalies associated with teleconnection patterns. It is not likely that the variability in EVI was caused by structural forest changes since no major disturbances or significant changes in biomass or species composition occurred during the last eight years. The infrared band in the EVI calculation is sensitive to changes in soil moisture which is one possible cause of EVI variability in forest canopies. Although we do not expect this to be the case at Wind River because high biomass will reduce the impact of the soil moisture signal on the overall EVI. In fact, an earlier remote sensing study at Wind River using 2001-2003 MODIS water indices showed that seasonal water content of this forest follows a similar trajectory to the tower-based NEP measurements (Cheng *et al.*, 2007). These results, in addition to our study, show the potential for using MODIS water and vegetation indices to identify landscape-scale anomalies in old-growth carbon exchange during strong teleconnection events.

5. Conclusions

Recent high frequency variability in the PDO since 1998 gave us a unique opportunity to examine additive teleconnection influences on the forest ecosystem as both strong negative (1999 and 2000) and positive (2003 and 2005) in-phase teleconnection events occurred between the PDO, PNA and ENSO during our flux measurement period. This study presented novel results that compare prolonged weather patterns resulting from dominant teleconnection leading modes and their influence on mass exchange at an old growth forest. We found that variability of net carbon exchange and canopy processes for an old-growth forest in the Pacific Northwest can be linked to large-scale teleconnection patterns. The largest ecosystem anomalies in NEP, GPP, R_{eco}, LUE, WUE, and EVI occurred during strong, in-phase climate events. On the other hand, year-to-year changes in tower-based and MODIS-derived FPAR were small and insignificant. Structural changes in the old-growth canopy cannot explain the variability of net ecosystem carbon exchange at Wind River, unlike some younger (50 to 150 years old) forests where structural change and biotic response does play an important role in explaining NEP variability (Richardson *et al.*, 2007, Urbanski *et al.*, 2007).

Observations of CO_2, H_2O and energy fluxes during positive and negative teleconnection leading modes may allow us to estimate how biosphere-atmospheric exchanges will vary over annual to decadal time scales. Furthermore, the ability to predict high frequency climate variability has improved during the last decade as our understanding of teleconnection behavior also improves (Chen *et al.*, 2004). The results of our study suggest that increases in the frequency or duration of cool-phase Pacific teleconnection patterns will increase annual carbon sequestration in mature Pacific Northwest conifer forests. However, stronger and more frequent warm phases will likely decrease net carbon uptake if increases in respiration fluxes are greater than any subsequent increases in GPP. Such strong, warm phase events can be considered to be "natural experiments" for testing hypotheses related to possible climate change scenarios.

Acknowledgements

The authors would like to thank the researchers and staff at the Wind River Canopy Crane Research Facility (WRCCRF) for their hospitality and assistance throughout this project, including Dr. Ken Bible (U Washington), Mark Creighton and Annie Hamilton. Special thanks are given to our field technician Matt Schroeder. Additional gratitude goes to Drs. Susan Ustin and Ruth Reck (UC Davis), Eugenia Gonzalez (UC Davis), and Drs. Dennis Baldocchi and Rodrigo Vargas (UC Berkeley) for their technical advice and help in the preparation of this manuscript, and to the GCB reviewers and Editor for their helpful suggestions and critiques. This research was supported by the Office of Science (BER), US Department of Energy, through the Western Regional Center of the National Institute for Global Environmental Change (Cooperative Agreement NO. DE-FC03-90ER61010). Any opinions, findings and conclusions or recommendations expressed herein are those of the authors and do not necessarily reflect the view of the DOE. The Wind River Canopy Crane Research Facility is operated under joint sponsorship of the University of Washington and the USDA Forest Service/PNW Station and we acknowledge both for significant support. Lawrence Livermore National Laboratory is operated by Lawrence Livermore National Security, LLC, for the U.S. Department of Energy, National Nuclear Security Administration under Contract DE-AC52-07NA27344.

References

Anthoni PM, Unsworth MH, Law BE, Irvine J, Baldocchi DD, Van Tuyl S, Moore D (2002) Seasonal differences in carbon and water vapor exchange in young and old-growth ponderosa pine ecosystems. *Agricultural and Forest Meteorology*, **111**, 203-222.

Baldocchi DD (2008) 'Breathing' of the terrestrial biosphere: lessons learned from a global network of carbon dioxide flux measurements systems. *Australian Journal of Botany*, **56**, 1-26.

Barnston AG, Livezey RE (1987) Classification, seasonality and persistence of low-frequency atmospheric circulation patterns. *Monthly Weather Review*, **115**, 1083-1126.

Bell GD, Basist AN (1994) Seasonal climate summary: The global climate of December 1992 – February, 1993. Part 1: Warm ENSO conditions continue in the Tropical Pacific; California drought abates. *Journal of Climate*, **7**, 1581-1605.

Berbigier P, Bonnefond J-M, Mellmann P (2001) CO2 and water vapour fluxes for 2 years above EuroFlux forest site. *Agricultural and Forest Meteorology*, **108**, 183-197.

Betts RA, Cox PM, Collins M, Harris PP, Huntingford C, Jones CD (2004) The role of ecosystem-atmosphere interactions in simulated Amazonian precipitation decrease and forest dieback under global climate warming. *Theoretical and Applied Climatology*, **78**, 157-175.

Bony S, Lau KM, Sud YC (1997) Sea surface temperature and large-scale circulation influences on tropical greenhouse effect and cloud radiative forcing. *Journal of Climate*, **10**, 2055-2077.

Case MJ, Peterson DL (2005) Fine-scale variability in growth-climate relationships of Douglas-fir, North Cascade Range, Washington. *Canadian Journal of Forest Research*, **35**, 2743-2755.

Chen D, Cane MA, Kaplan A, Zebiak S, Huang D (2004) Predictability of El Niño over the past 148 years. *Nature*, **428**, 733-736.

Chen, JQ, Falk M, Euskirchen E *et al.* (2002) Biophysical controls of carbon flows in three successional Douglas-fir stands based on eddy-covariance measurements. *Tree Physiology*, **22**, 169-177.

Chen WY (1982) Fluctuations in Northern Hemisphere 700 mb height field associated with the Southern Oscillation. *Monthly Weather Review*, **110**, 808-823.

Cheng Y-B, Wharton S, Ustin SL, Zarco-Tejada PJ, Falk M, Paw U KT (2007) Relationships between Moderate Resolution Imaging Spectroradiometer water indexes and tower flux data in an old-growth conifer forest. *Journal of Applied Remote Sensing*, **1**, 013513.

Chuck A, Tyrrell T, Totterdell IJ, Holligan PM (2005) The oceanic response to carbon emissions over the next century: investigation using three ocean carbon cycle models. *Tellus Series B – Chemical and Physical Meteorology*, **57**, 70-86.

Clark DA, Piper SC, Keeling CD, Clark DB (2003) Tropical rain forest tree growth and atmospheric carbon dynamics linked to interannual temperature variation during 1984-2000. *Proceedings of the National Academy of Science*, **100**(10), 5852-5857.

Cox PM, Betts RA, Collins M, Harris PP, Huntingford C, Jones CD (2004) Amazonian forest dieback under climate-carbon cycle projections for the 21st century. *Theoretical and Applied Climatology*, **78**, 137-156.

DeBell DS, Franklin JF (1987) Old-growth Douglas-fir and western hemlock: a 36-year record of growth and mortality. *Western Journal of Applied Forestry*, **2**, 111-114.

Desai AR, Bolstad PV, Cook BD, Davis KJ, Carey EV (2005) Comparing net ecosystem exchange of carbon dioxide between an old-growth and mature forest in the upper Midwest, USA. *Agricultural and Forest Meteorology*, **128**, 33-55.

Dunn AL, Barford CC, Wofsy SC, Goulden ML, Daube BC (2007) A long-term record of carbon exchange in a boreal black spruce forest: means, responses to interannual variability, and decadal trends. *Global Change Biology*, **13**, 577-590.

Esbenson SK (1984) A comparison of intermonthly and interannual teleconnections in the 700mb geopotential height field during the Northern Hemisphere winter. *Monthly Weather Review*, **112**, 2016-2032.

Falk M (2005) *Carbon and energy exchange between an old-growth forest and the atmosphere*. PhD Dissertation, University of California, Davis, 216 pp.

Falk M, Paw U KT, Wharton S, Schroeder M (2005) Is soil respiration a major contributor to the carbon budget within a Pacific Northwest old-growth forest? *Agricultural and Forest Meteorology*, **135**, 269-283.

Falk M, Wharton S, Schroeder M, Ustin S, Paw U KT (2008) Flux partitioning in an old growth forest: seasonal and interannual dynamics. *Tree Physiology*, **28**, 509-520.

Franklin JF, Waring RH (1980) Distinctive features of the northwestern conifer forest: development, structure and function. In: *Forests: fresh perspectives from ecosystem analysis* (ed. Waring RH), pp. 59-86, Oregon State University Press, Corvallis, Oregon.

Franklin JF, DeBell, DS (1988) Thirty-six years of tree population changes in an old-growth *Pseudotsuga-Tsuga* forest. *Canadian Journal of Forest Research*, **18**, 633-639.

Gedalof Z, Smith DJ (2001) Interdecadal climate variability and regime-scale shifts in Pacific North America. *Geophysical Research Letters*, **28**, 1515-1518.

Goldstein A, Hultman N, Fracheboud J *et al.* (2000) Affects of climate variability on the carbon dioxide, water and sensible heat fluxes above a ponderosa plantation in the Sierra Nevada (CA). *Agricultural and Forest Meteorology*, **101**, 113-129.

Goulden ML, Munger JW, Fan SM, Daube BC, Wofsy SC (1996) Measurements of carbon sequestration by long-term eddy covariance: Methods and a critical evaluation of accuracy. *Global Change Biology*, **2**,169-182.

Gower ST, Kucharik CJ, Norman JM (1999) Direct and indirect estimation of leaf area index, fAPAR, and net primary production of terrestrial ecosystems. *Remote Sensing of the Environment*, **70**, 29-51.

Graumlich LJ, Brubaker LB, Grier CC (1989) Long-term trends in forest net primary productivity - Cascade Mountains, Washington. *Ecology*, **70**, 405-410.

Harmon ME, Bible K, Ryan MG, Shaw DC, Chen H, Klopatek J, Li X (2004) Production, respiration, and overall carbon balance in an old-growth *Pseudotsuga-tsuga* forest ecosystem. *Ecosystems*, **7**, 498-512.

Hollinger DY, Kelliher FM, Byers JN, Hunt JE, McSeveny TM, Weir PL (1994) Carbon-dioxide exchange between an undisturbed old-growth temperate forest and the atmosphere. *Ecology*, **75**, 134-150.

Huete A, Justice C, van Leeuwen W (1999) MODIS Vegetation Index (MOD13) Algorithm Theoretical Basis Document, Version 3.0, NASA Goddard Space Flight Center, Greenbelt, MD 20771, USA. Available on-line at http://modis.gsfc.nasa.gov/data/atbd_mod13.pdf

Humphreys ER, Black TA, Morgenstern K, Cai T, Drewitt GB, Nesic Z, Trofymow JA (2006) Carbon dioxide fluxes in coastal Douglas-fir stands at different stages of development after clearcut harvest. *Agricultural and Forest Meteorology*, **140**, 6-22.

Hurrell JW (1995) Decadal trends in the North Atlantic Oscillation: Regional temperatures and precipitation. *Science*, **269**, 676-679.

Hurrell JW (1996) Influence of variations in extratropical wintertime teleconnections on Northern Hemisphere temperatures. *Geophysical Research Letters*, **23**, 665-668.

Janssens IA, Lankreijer H, Matteucci G *et al.* (2001) Productivity overshadows temperature in determining soil and ecosystem respiration across European forests. *Global Change Biology*, **7**, 269-278.

Knohl A, Schulze ED, Kolle O, Buchmann N (2003) Large carbon uptake by an unmanaged 250-year-old deciduous forest in Central Germany. *Agricultural and Forest Meteorology*, **118**, 151-167.

Knyazikhin Y, Glassy J, Privette J *et al.* (1999) MODIS leaf area index (LAI) and fraction of photosynthetically active radiation absorbed by vegetation (FPAR) product (MOD15) algorithm. Theoretical Basis Document, Version 4.0, NASA Goddard Space Flight Center, Greenbelt, MD 20771, USA. Available on-line at http://modis.gsfc.nasa.gov/data/atbd/atbd_mod15.pdf

Law BE, Williams M, Anthoni PM, Baldocchi DD, Unsworth MH (2000) Measuring and modelling seasonal variation of carbon dioxide and water vapour exchange of a *Pinus ponderosa* forest subject to soil water deficit. *Global Change Biology*, **6**, 613-630.

Law BE, Falge E, Gu L *et al.* (2002) Environmental controls over carbon dioxide and water vapor exchange of terrestrial vegetation. *Agricultural and Forest Meteorology*, **113**, 97-120.

Law BE, Sun OJ, Campbell J, van Tuyl S, Thornton PE (2003) Changes in carbon storage and fluxes in a chronosequence of ponderosa pine. *Global Change Biology*, **9**, 510-524.

Law BE, Turner D, Campbell J, Sun OJ, van Tuyl S, Ritts WD, Cohen WB (2004) Disturbance and climate effects on carbon stocks and fluxes across Western Oregon USA. *Global Change Biology*, 10, 1429-1444.

Lemon ER (1969) Important microclimatic factors in soil-water-plant relationships. *Modifying the Soil and Water Environment for Approaching the Agricultural Potential of the Great Plains*. Great Plains Agr. Council Publ. No. 3, pp. 95-102.

Lee XH, Fuentes JD, Staebler RM, Neumann HH (1999) Long-term observation of the atmospheric exchange of CO2 with a temperate deciduous forest in southern Ontario, Canada. *Journal of Geophysical Research*, **104**(D13), 15975-15984.

Loescher HW, Oberbauer SF, Gholz HL, Clark DB (2003) Environmental controls on net ecosystem-level carbon exchange and productivity in a Central American tropical wet forest. *Global Change Biology*, **9**, 396-412.

Loomis RS, Williams WA (1963) Maximum crop productivity: An estimate. *Crop Science*, **3**, 67-72.

Luyssaert S, Janssens IA, Sulkava M *et al.* (2007) Photosynthesis drives anomalies in net carbon-exchange of pine forests at different latitudes. *Global Change Biology*, **13**, 2110-2127.

McCabe GJ, Dettinger MD (1999) Decadal variations in the strength of ENSO teleconnections with precipitation in the western United States. International *Journal of Climatology*, **19**, 1399-1410.

Mantua NJ, Hare SR, Zhang Y, Wallace JM, Francis RC (1997) A Pacific interdecadal climate oscillation with impacts on salmon production. *Bulletin of the American Meteorological Society*, **78**, 1069-1079.

Mantua NJ, Hare SR (2002) The Pacific decadal oscillation. *Journal of Oceanography*, **58**, 35-44.

Monteith JL (1972) Solar radiation and production in tropical ecosystems. *Journal of Applied Ecology*, **9**, 747-766.

Monteith JL (1977) Climate and the efficiency of crop production in Britain. *Philosophical Transactions of the Royal Society* B, **281**, 277-294.

Morgenstern K, Black TA, Humphreys ER *et al.* (2004) Sensitivity and uncertainty of the carbon balance of a Pacific Northwest Douglas-fir forest during an El Niño La Niña cycle. *Agricultural and Forest Meteorology*, **123**, 201-219.

Mote PW, Parson E, Hamlet AF *et al.* (2003) Preparing for climatic change: The water, salmon, and forests of the Pacific Northwest. *Climatic Change*, **61**, 45-88.

Myneni R, Hoffman S, Knyazikhin Y *et al.* (2002) Global products of vegetation leaf area and fraction of absorbed PAR from year one of MODIS data. *Remote Sensing of Environment*, **83**, 214-241.

Oak Ridge National Laboratory Distributed Active Archive Center (ORNL-DAAC) (2008) MODIS subsetted land products, Collection 5. Available on-line [http://daac.ornl.gov/MODIS/] from ORNL-DAAC, Oak Ridge, Tennessee, USA. Accessed July 1, 2008.

Odum EP (1965) *Fundamentals of Ecology*, 2nd ed. Philadelphia: Saunders.

Parker GG, Davis MM, Chapotin SM (2002) Canopy light transmittance in Douglas-fir/western hemlock stands. *Tree Physiology*, **22**, 147-157.

Parker GG, Harmon ME, Lefsky MA *et al.* (2004) Three-dimensional structure of an old-growth *Pseudotsuga-tsuga* canopy and its implications for radiation balance, microclimate, and gas exchange. *Ecosystems*, **7**, 440-453.

Paw U KT, Baldocchi DD, Meyers TP, Wilson KB (2000) Correction of eddy-covariance measurements incorporating both advective effects and density fluxes. *Boundary-Layer Meteorology*, **97**, 487-511.

Paw U KT, Falk M, Suchanek TH *et al.* (2004) Carbon dioxide exchange between an old-growth forest and the atmosphere. *Ecosystems*, **7**, 513-524.

Pilegaard K, Mikkelsen TN, Beier C, Jensen NO, Ambus P, Ro-Poulsen H (2003) Field measurements of atmosphere-biosphere interactions in a Danish beech forest. *Boreal Environment Research*, **8**, 315-333.

Rahman AF, Sims DA, Cordova VD, El-Masri BZ (2005) Potential of MODIS EVI and surface temperature for directly estimating per-pixel ecosystem C fluxes. *Geophysical Research Letters*, **32**, L19404, doi:10.1029/2005GL024127.

Reichstein M, Falge E, Baldocchi D *et al.* (2005) On the separation of net ecosystem exchange into assimilation and ecosystem respiration: review and improved algorithm. *Global Change Biology*, **11**, 1424-1439.

Reichstein M, Ciais P, Papale D *et al.* (2007) Reduction of ecosystem productivity and respiration during the European summer 2003 climate anomaly: a joint flux tower, remote sensing and modeling analysis. *Global Change Biology*, **13**, 634-651.

Richardson AD, Hollinger DY, Aber JD, Ollinger SV, Braswell BH (2007) Environmental variation is directly responsible for short- but not long-term variation in forest-atmosphere carbon exchange. *Global Change Biology*, **13**, 788-803.

Rocha AV, Goulden ML, Dunn AL, Wofsy SC (2006) On linking interannual tree ring variability with observations of whole-forest CO2 flux. *Global Change Biology*, **12**, 1378-1389.

Rosenberg NJ, Blad BL, Verma SB (1983) *Microclimate, The Biological Environment,* 2nd edition, pp. 495, John Wiley & Sons, New York.

Schimel D, Melillo J, Tian H *et al.* (2000) Contribution of increasing CO2 and climate to carbon storage by ecosystems in the United States. *Science*, **287**, 2004-2006.

Schulze ED (1986) Carbon dioxide and water vapour exchange in response to drought in the atmosphere and in the soil. *Annual Review of Plant Physiology*, **37**, 247-274.

Schwalm CR, Black TA, Morgenstern K, Humphreys ER (2007) A method for deriving net primary productivity and component respiratory fluxes from tower-based eddy covariance data: a case study using a 17-year data record from a Douglas-fir chronosequence. *Global Change Biology*, **13**, 370-385.

Schwarz PA, Law BE, Williams M, Irvine J, Kurpius M, Moore D (2004) Climatic versus biotic constraints on carbon and water fluxes in seasonally drought-affected ponderosa pine ecosystems. *Global Biogeochemical Cycles*, **18**, GB4007, doi: 10.1029/2004GB002234.

Shaw DC, Franklin JF, Bible K, Klopatek J, Freeman E, Greene S, Parker GG (2004) Ecological setting of the Wind River old-growth forest. *Ecosystems*, **7**, 427-439.

Smithwick EA, Harmon ME, Remillard SM, Acker SA, Franklin JF (2002) Potential upper bounds of carbon stores of forests in the Pacific Northwest. *Ecological Applications*, **12**, 1303-1317.

Swinbank WC (1951) Measurement of vertical transfer of hear and water vapor by eddies in the lower atmosphere. *Journal of Meteorology*, **8**, 135-145.

Thomas SC, Winner WE (2000) Leaf area index of an old-growth Douglas-fir forest estimated from direct structural measurements in the canopy. *Canadian Journal of Forest Research*, **30**, 1922-1930.

Thornton PE, Law BE, Gholz HL *et al.* (2002) Modeling and measuring the effects of disturbance history on carbon and water budgets in evergreen needleleaf forests. *Agricultural and Forest Meteorology*, **113**, 185-222.

Tian YC, Woodcock Y, Wang J *et al.* (2002) Multiscale analysis and validation of the MODIS LAI product 1. Uncertainty assessment. *Remote Sensing of Environment*, **83**, 414-430.

Trofymow JA, Stinson G, Kurz WA (2008) Derivation of a spatially explicit 86-year retrospective carbon budget for a landscape undergoing conversion from old-growth to managed forest on Vancouver Island, BC. *Forest Ecology and Management*, **256**, 1677-1691.

Turner DP, Koerper GJ, Harmon ME, Lee JJ (1995) A carbon budget for forests of the conterminous United States. *Ecological Applications*, **5**, 421-436.

Turner DP, Ritts WD, Cohen WB *et al.* (2005) Site-level evaluation of satellite-based global terrestrial gross primary production and net primary production monitoring. *Global Change Biology*, **11**, 666-684.

Urbanski S, Barford C, Wofsy S *et al.* (2007) Factors controlling CO2 exchange on timescales from hourly to decadal at Harvard Forest. *Journal of Geophysical Research*, **112**, G02020, doi:10.1029/2006JG000293.

Valentini R, Matteucci G, Dolman AJ *et al.* (2000) Respiration as the main determinant of carbon balance in European forests. *Nature*, **404**, 861-865.

van Loon H, Rogers, JC (1981) The Southern Oscillation, Part 1: Global associations with pressure and temperature in Northern winter. *Monthly Weather Review*, **109**, 1150-1162.

Wallace JM, Gutzler DS (1981) Teleconnections in the geopotential height field during the Northern Hemispheric winter. *Monthly Weather Review*, **109**, 784-812.

Wolter K, Timlin MS (1993) Monitoring ENSO in COADS with a seasonally adjusted principal component index. *Proc. of the 17th Climate Diagnostics Workshop*, Norman, OK, NOAA/NMC/CAC, NSSL, Oklahoma Clim. Survey, CIMMS and the School of Meteor., Univ. of Oklahoma, 52-57.

Wolter K, Timlin MS (1998) Measuring the strength of ENSO events: How does 1997/1998 rank? *Weather*, **53**, 315-324.

Tables

Name	Years used	Time resolution	Definition	Data source	Reference
PDO	1950-2007	Monthly, annual	Leading PC from an un-rotated EOF analysis of monthly residual North Pacific SST anomalies	http://jisao.washington.edu/pdo/PDO.latest	Mantua *et al.*, 1997
PNA	1950-2007	Daily, monthly, annual	Leading eigenvector from a rotated PCA based on the 700 hPa height field in the North Pacific	ftp://ftp.cpc.ncep.noaa.gov/wd52dg/data/indices/tele_index.nh	Wallace & Gutzler, 1981
MEI	1950-2007	Bimonthly, annual	First PC of six observed variables (SLP, zonal and meridional component of surface wind, SST, surface air temperature, total cloudiness fraction) over the tropical Pacific	http://www.cdc.noaa.gov/people/klaus.wolter/MEI/table.html	Wolter & Timlin, 1993, 1998

Table 1 Methodology and references for the Pacific Ocean climate indices. PC = principal component, PCA = principal component analysis, EOF = empirical orthogonal function, SST = sea surface temperature, SLP = sea level pressure.

	PDO – PNA – MEI –	PDO – PNA – MEI +	PDO – PNA + MEI –	PDO – PNA + MEI +	PDO + PNA – MEI –	PDO + PNA – MEI +	PDO + PNA+ MEI –	PDO + PNA + MEI +
Frequency	16	7	5	5	6	1	4	14
Flux Years	1999, 2000		2002	2007	2006		2001	2003, 2004, 2005

Table 2 The frequency of occurrence for the eight climate-phase combinations for the historical data record (1950-2007) and during the flux measurement period (1999-2007).

	Negative Phase			Positive Phase		
	PDO	PDO & PNA	PDO & PNA & MEI	PDO	PDO & PNA	PDO & PNA & MEI
water-year precipitation (mm)	2596	2762	2971	2117	1960	2069
dry season precipitation (mm)	130	150	171	110	123	125
annual mean temperature (ºC)	8.69	8.50	7.90	8.84	8.82	8.90
rainy season temperature (ºC)	3.34	3.36	3.12	3.76	3.53	3.87
dry season temperature (ºC)	16.61	16.71	15.91	16.55	16.62	16.84
NEP (g C m^{-2} $year^{-1}$) (± uncertainty)	+ 130 (±53)			- 57 (±38)		

Table 3 Additive effects of PDO, the in-phase PDO and PNA, and the in-phase PDO, PNA and MEI on historical local climate (1951-2007) and tower NEP (1999-2007) data. Weak phases of El Niño/La Niña and PNA are considered phase-neutral and those years were not included. The rainy season is defined as October through March; dry season is July through September. Uncertainty in NEP was estimated from an error analysis of random and systematic errors in the eddy covariance data.

Independent variable	Dependent variable	Time resolution	n	R^2	r	P
CCI	precipitation	annual	57	0.18	-0.41	$P < 0.01$
CCI	temperature	annual	57	0.05	0.28	$P > 0.01$
CCI	NEP	annual	9	0.55	-0.71	$P < 0.01$
		monthly	83	0.34	-0.59	$P < 0.001$
CCI	GPP	annual	8	0.64	0.78	$P > 0.01$
		monthly	76	0.22	0.47	$P < 0.001$
CCI	R_{eco}	annual	8	0.75	0.83	$P < 0.01$
		monthly	76	0.33	0.53	$P < 0.001$
CCI	EVI	monthly	44	0.28	-0.49	$P < 0.001$
ΔEVI	ΔNEP	monthly	44	0.34	0.52	$P < 0.001$

Table 4. Linear model statistics including number of data points, adjusted coefficient of determination (R^2), Spearman correlation coefficient (r) and ANOVA p-value show significant relationships between nearly all of the CCI, tower flux and MODIS EVI measurements.

Figure Legends

Fig. 1 Time series plot of standardized precipitation anomalies (bars) (a) and standardized temperature anomalies (bars) (b) from the Wind River region (1950-2007) in comparison to the annual MEI, PNA and PDO indices.

Fig. 2 The frequency of annual Composite Climate Index magnitudes from 1950 to 2007 with the flux measurement years labeled.

Fig. 3 Time series of the annual MEI (a), PNA (b), PDO (c) and CCI (d) from 1950-2007 and NEP measurements from 1999-2007. Positive magnitudes indicate warm climate phases and net carbon source years. Negative magnitudes indicate cool climate phases and net carbon sink years.

Fig. 4 Monthly average air temperature (a) and vapor pressure deficit (b) associated with positive (warm), negative (cool), and neutral climate phases from 1999-2007.

Fig. 5 Greater net carbon uptake is associated with more negative annual CCI ($R^2 = 0.55$, $P < 0.01$) (a). Monthly anomalies in NEP show more scatter ($R^2 = 0.34$) but are significantly correlated ($P < 0.001$) to the CCI (b).

Fig. 6 Annual (a, $R^2 = 0.64$, $P > 0.01$) and monthly (b, $R^2 = 0.22$, $P < 0.001$) GPP anomalies are positively related to the CCI. Higher photosynthesis was observed during positive climate phases.

Fig. 7 Annual (a, $R^2 = 0.75$, $P < 0.01$) and monthly (b, $R^2=0.33$, $P < 0.001$) R_{eco} anomalies are positively related to the CCI. Reduced ecosystem respiration was observed during negative climate phases.

Fig. 8 Monthly integrated NEP associated with the three dominant climate phases. The black box highlights the seasonal transition from net carbon sink to net carbon source (e.g., where the summer-time NEP crosses zero). This occurs in late May for positive or warm phase years, mid-June for neutral phase years, and mid-July for negative or cool phase years.

Fig. 9a Monthly mean midday WUE during positive (warm) and negative (cool) climate phases. Largest climate-phase WUE differences occur during the summer months. Fig. 9b Monthly LUE during positive (warm) and negative (cool) phase for all midday hours regardless of sky condition. Rainy season months have been excluded from the figures.

Fig. 10 Monthly time series plot of the Composite Climate Index (a) and the MODIS-derived EVI from 1999 (MODIS starts in 2000) through 2007 (b). The large triangles are annual mean growing season EVI.

Fig. 11 Monthly growing season EVI (2000-2007) is negatively related ($R^2 = 0.28$, $P < 0.001$) to the monthly CCI (a). The relationship between monthly NEP anomalies (2000-2007) and monthly EVI anomalies is significant ($R^2 = 0.34$, $P < 0.001$) and higher EVI is generally associated with greater net carbon uptake (b). Note that the sign notation in Fig. 11b has been switched on the x-axis so that positive values are on the left hand side of the y-axis and negative values are on the right hand side.

Figures

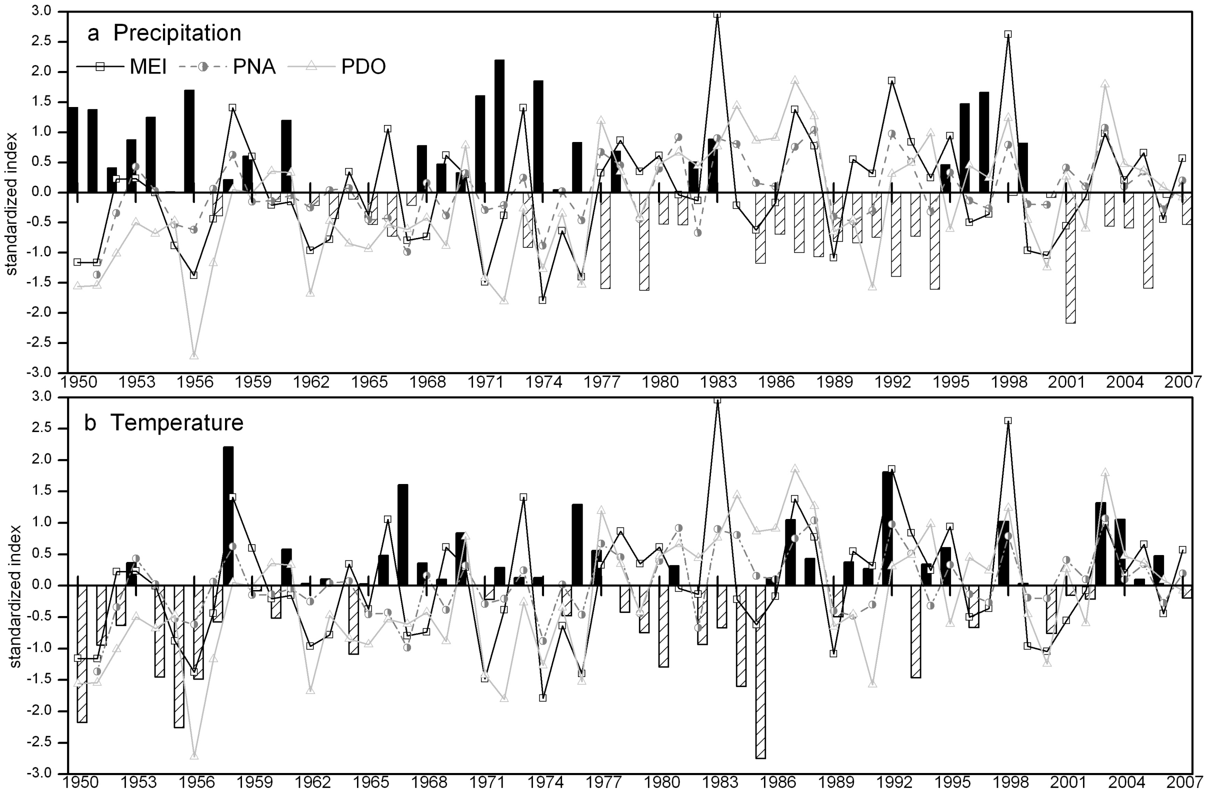

Fig. 1

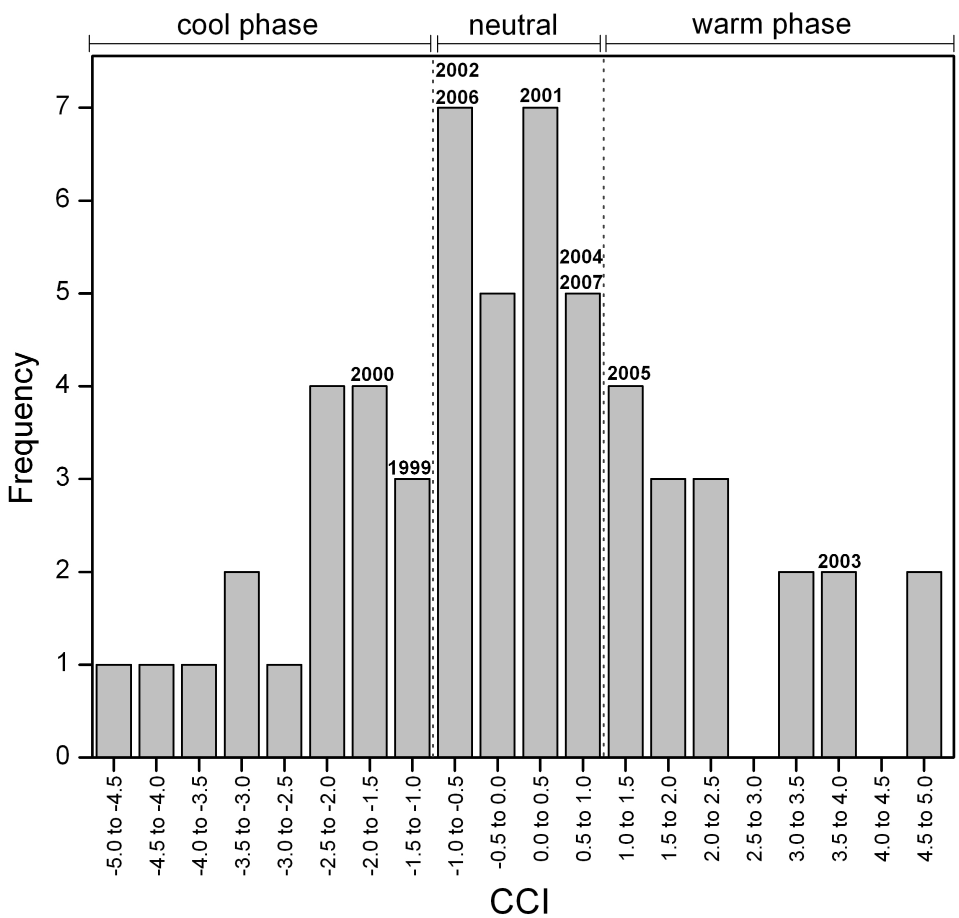

cool phase
neutral
warm phase
Frequency
CCI
0
1
2
3
4
5
6
7
2002
2006
2001
2004
2007
2000
1999
2005
2003
-5.0 to -4.5
-4.5 to -4.0
-4.0 to -3.5
-3.5 to -3.0
-3.0 to -2.5
-2.5 to -2.0
-2.0 to -1.5
-1.5 to -1.0
-1.0 to -0.5
-0.5 to 0.0
0.0 to 0.5
0.5 to 1.0
1.0 to 1.5
1.5 to 2.0
2.0 to 2.5
2.5 to 3.0
3.0 to 3.5
3.5 to 4.0
4.0 to 4.5
4.5 to 5.0

Fig. 2

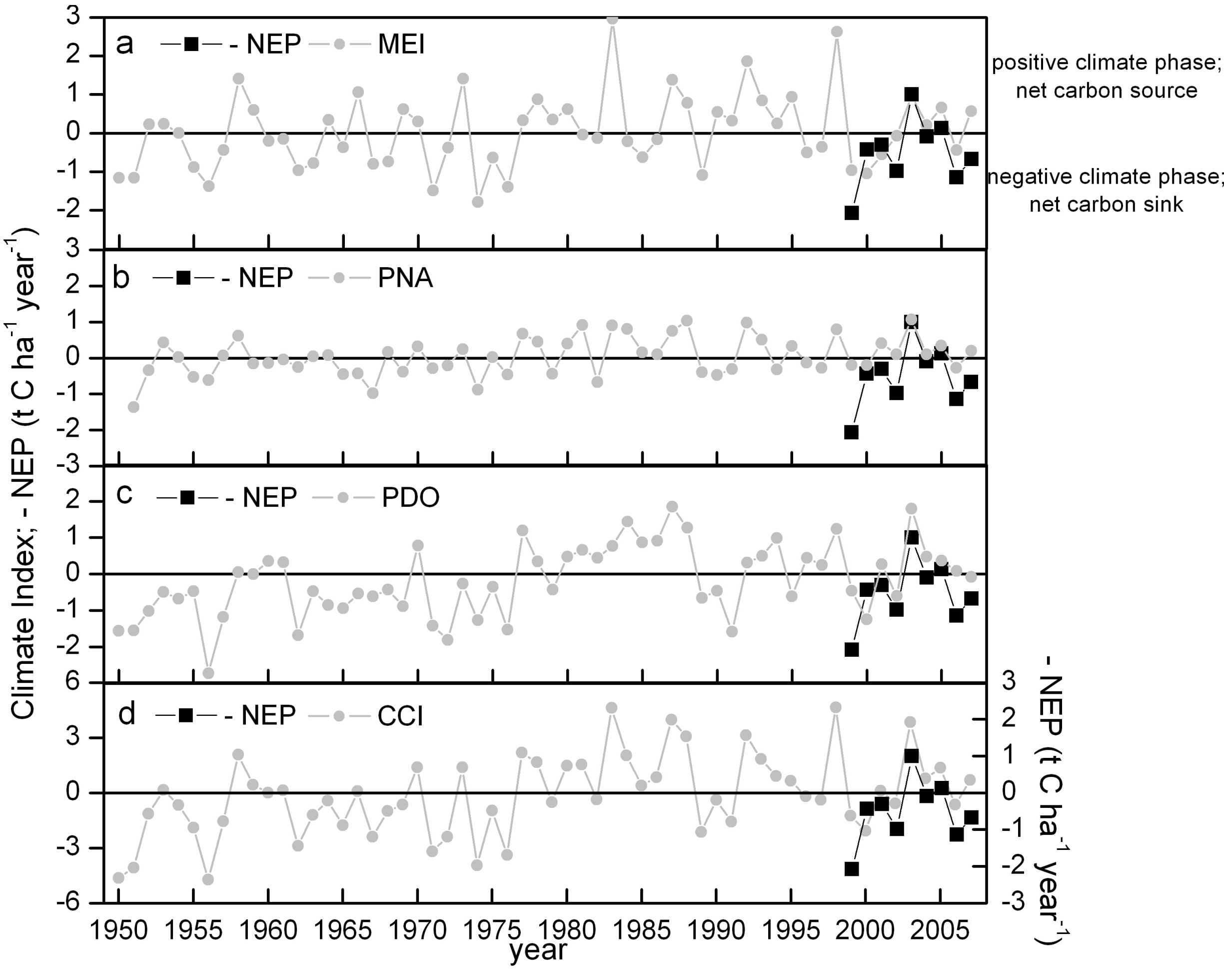
a
- NEP
MEI
positive climate phase;
net carbon source
negative climate phase;
net carbon sink
b
- NEP
PNA
c
- NEP
PDO
d
- NEP
CCI
Climate Index; - NEP (t C ha^{-1} year^{-1})
- NEP (t C ha^{-1} year^{-1})
year
1950
1955
1960
1965
1970
1975
1980
1985
1990
1995
2000
2005

Fig. 3

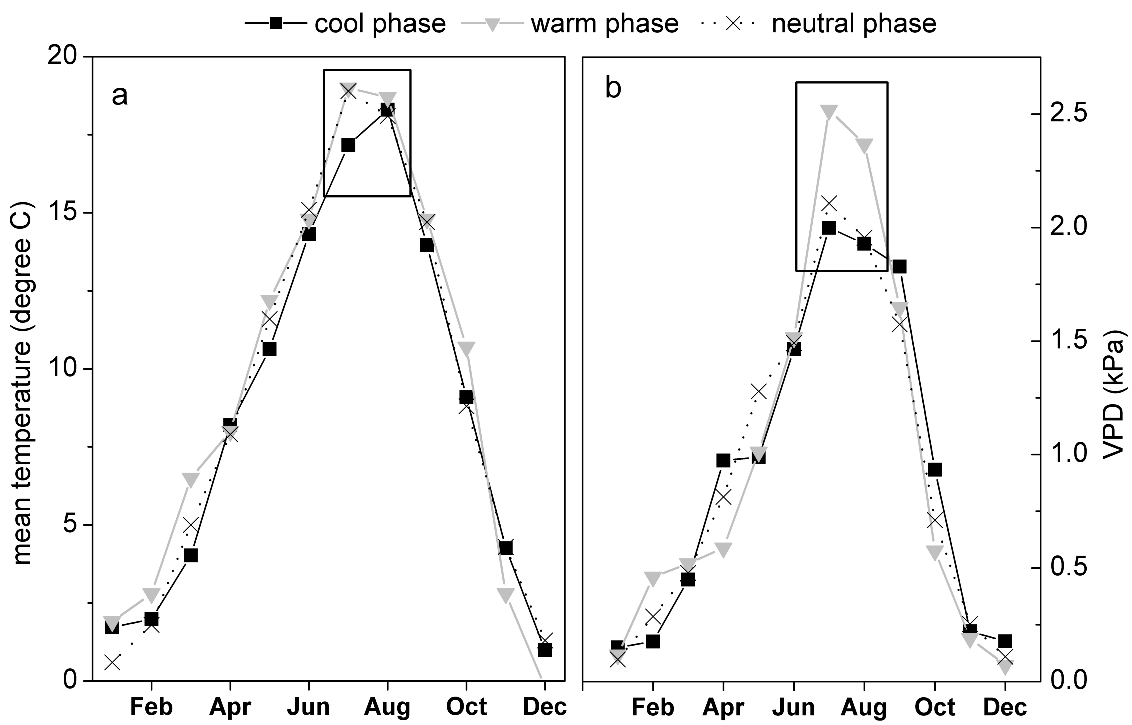
cool phase
warm phase
neutral phase
a
b
mean temperature (degree C)
VPD (kPa)
0
5
10
15
20
0.0
0.5
1.0
1.5
2.0
2.5
Feb
Apr
Jun
Aug
Oct
Dec

Fig. 4

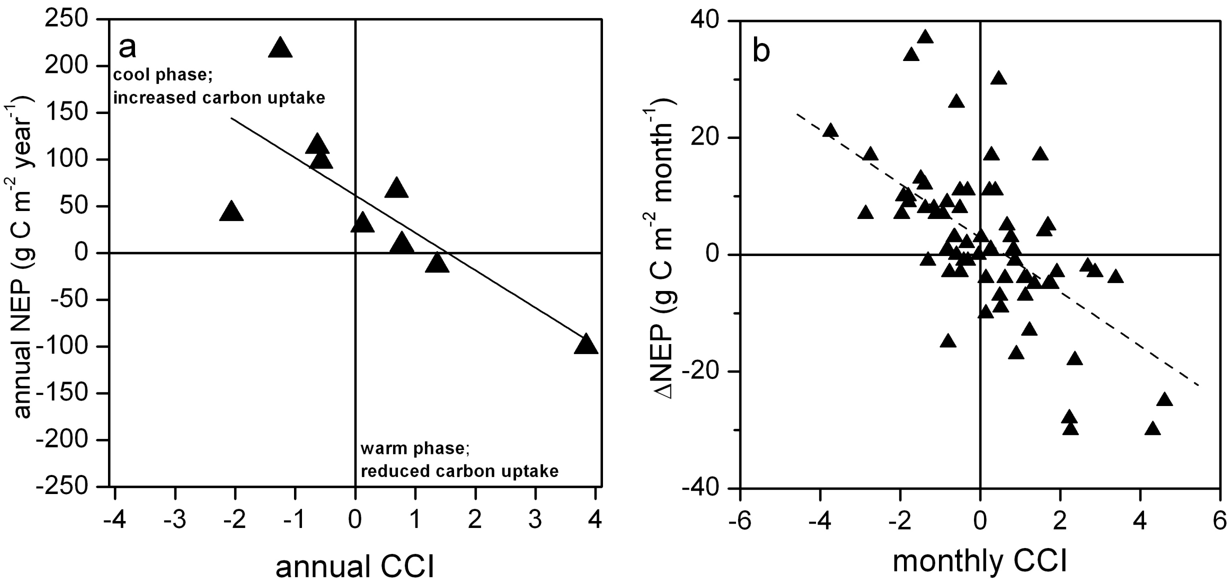
a
cool phase;
increased carbon uptake
warm phase;
reduced carbon uptake
annual NEP (g C m-2 year-1)
annual CCI
b
ΔNEP (g C m-2 month-1)
monthly CCI

Fig. 5

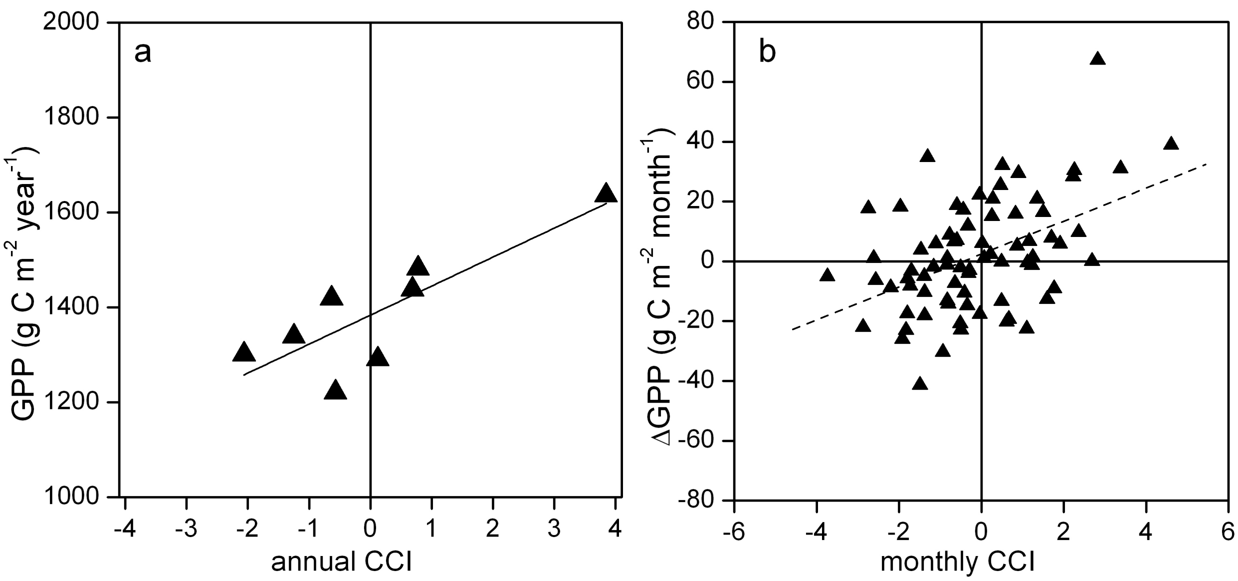
a
GPP (g C m-2 year-1)
2000
1800
1600
1400
1200
1000
-4 -3 -2 -1 0 1 2 3 4
annual CCI
b
ΔGPP (g C m-2 month-1)
80
60
40
20
0
-20
-40
-60
-80
-6 -4 -2 0 2 4 6
monthly CCI

Fig. 6

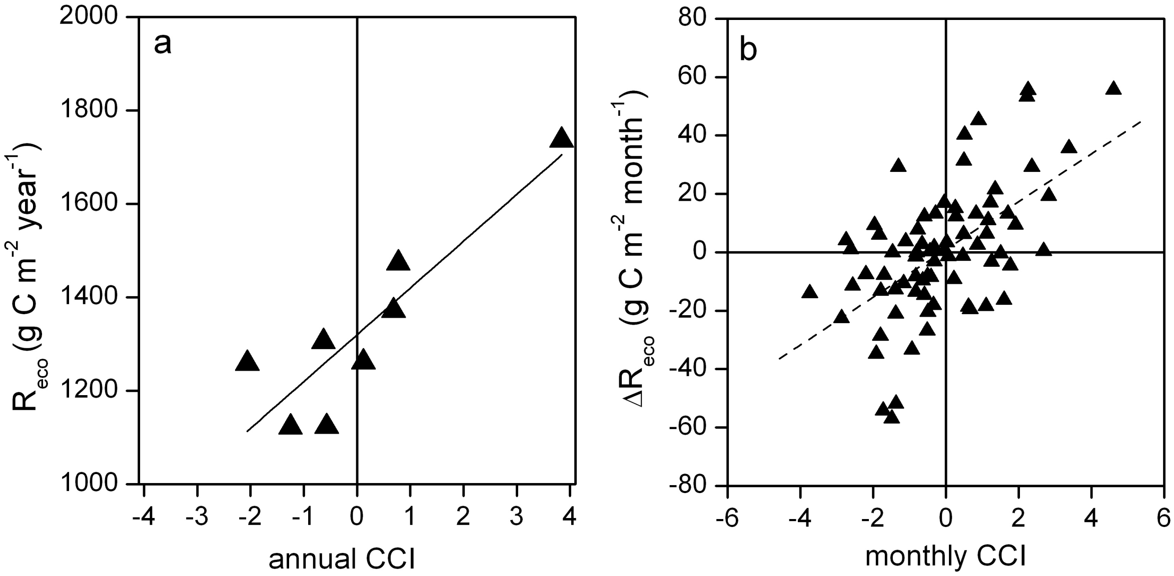
a
b
R_{eco} (g C m^{-2} $year^{-1}$)
annual CCI
ΔR_{eco} (g C m^{-2} $month^{-1}$)
monthly CCI

Fig. 7

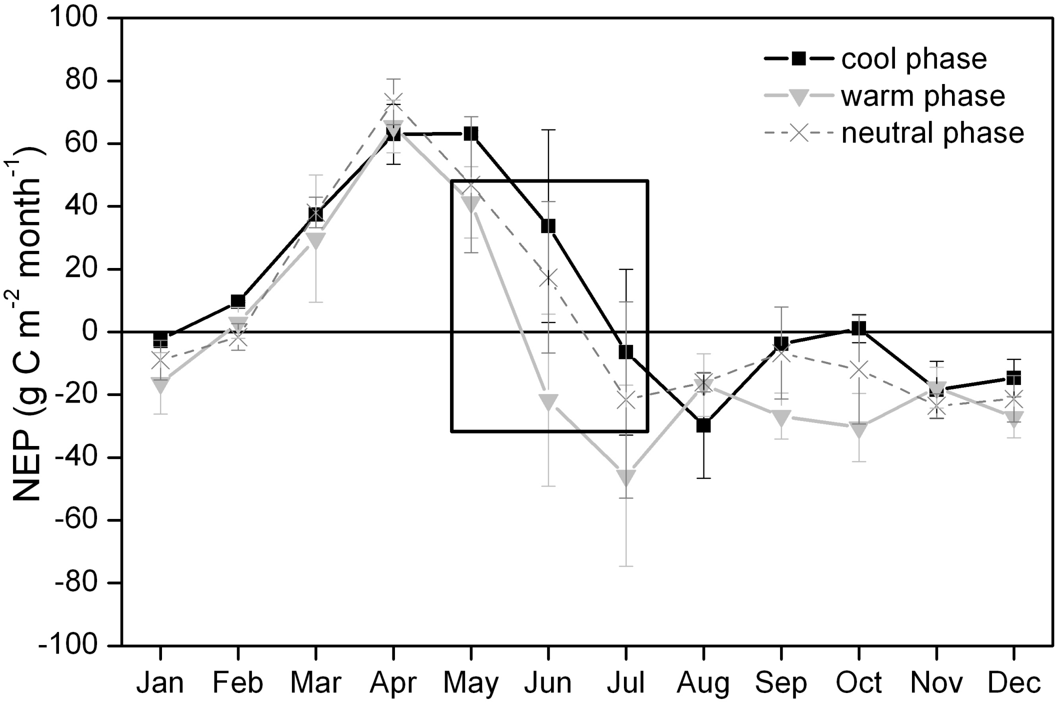
cool phase
warm phase
neutral phase
NEP (g C m-2 month-1)
100
80
60
40
20
0
-20
-40
-60
-80
-100
Jan
Feb
Mar
Apr
May
Jun
Jul
Aug
Sep
Oct
Nov
Dec

Fig. 8

1

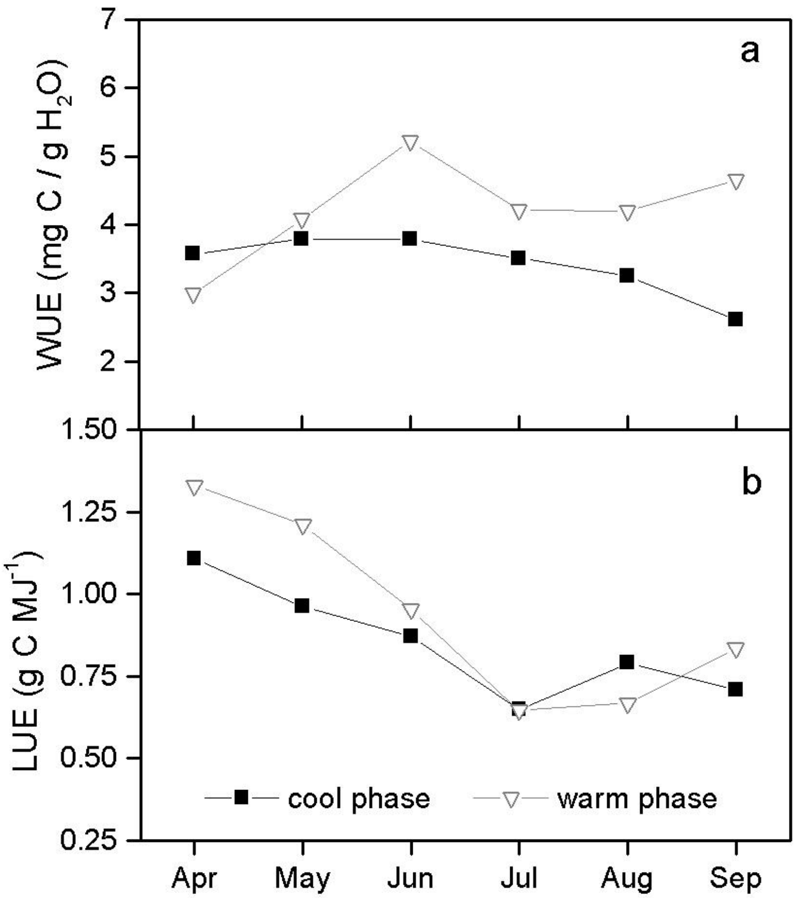

a
b
WUE (mg C / g H_2O)
LUE (g C MJ^{-1})
7
6
5
4
3
2
1.50
1.25
1.00
0.75
0.50
0.25
cool phase
warm phase
Apr
May
Jun
Jul
Aug
Sep

2

3 **Fig. 9**

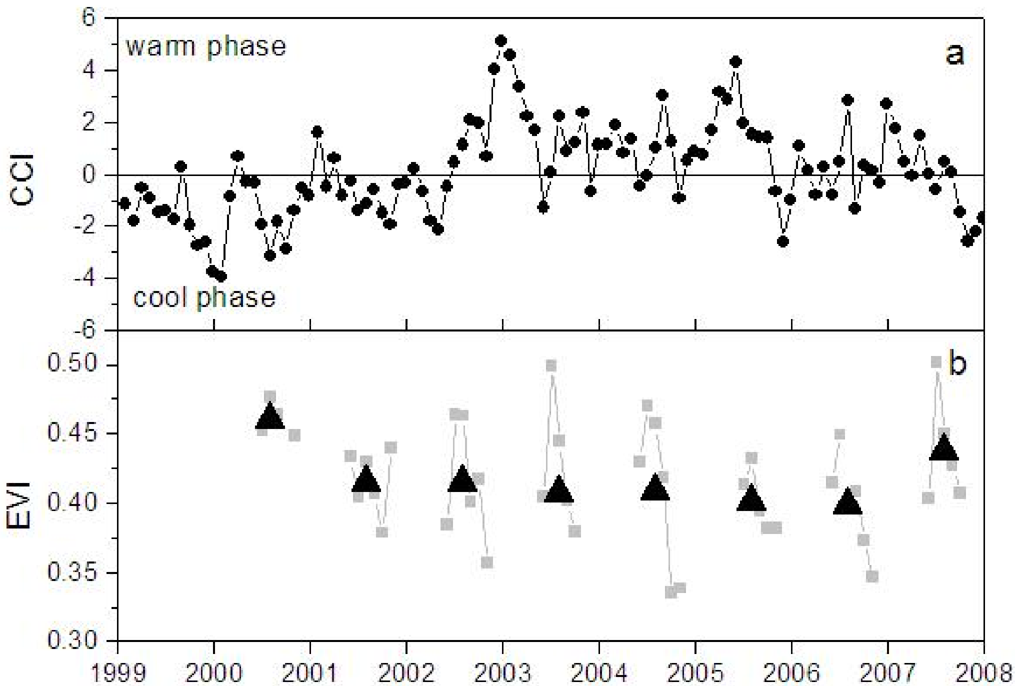
warm phase
a
cool phase
CCI
6
4
2
0
-2
-4
-6
b
EVI
0.50
0.45
0.40
0.35
0.30
1999
2000
2001
2002
2003
2004
2005
2006
2007
2008

Fig. 10

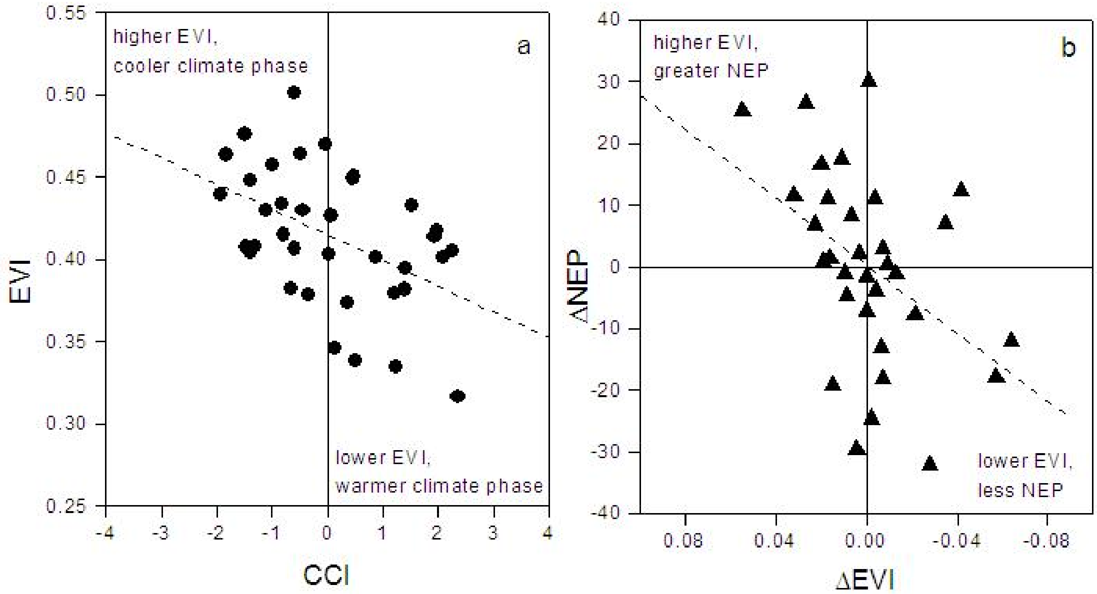

higher EVI,
cooler climate phase
a
lower EVI,
warmer climate phase
EVI
CCI
0.55
0.50
0.45
0.40
0.35
0.30
0.25
-4
-3
-2
-1
0
1
2
3
4
higher EVI,
greater NEP
b
lower EVI,
less NEP
ΔNEP
ΔEVI
40
30
20
10
0
-10
-20
-30
-40
0.08
0.04
0.00
-0.04
-0.08

1

2 **Fig. 11**

3